

1 Immediate and long-lasting impacts of the Mt. Pinatubo 2 eruption on ocean oxygen and carbon inventories

3 **Amanda R. Fay¹, Galen A. McKinley¹, Nicole S. Lovenduski^{2,3}, Yassir Eddebbar⁴, Michael
4 N. Levy⁵, Matthew C. Long⁵, Holly C. Olivarez^{3,6}, Rea R. Rustagi¹**

5 ¹Columbia University and Lamont-Doherty Earth Observatory, Palisades, NY, USA

6 ²Department of Atmospheric and Oceanic Sciences, University of Colorado, Boulder, CO, USA

7 ³Institute of Arctic and Alpine Research, University of Colorado, Boulder, CO, USA

8 ⁴Scripps Institution of Oceanography, University of California San Diego, La Jolla, CA, USA

9 ⁵Climate and Global Dynamics Laboratory, National Center for Atmospheric Research, Boulder, CO, USA

10 ⁶Department of Environmental Studies, University of Colorado, Boulder, CO, USA

11 **Key Points:**

- 12 • Two initial-condition large ensembles are used to quantify the ocean physical and bio-
geochemical response to the 1991 eruption of Mt. Pinatubo
- 13 • Oxygen is immediately absorbed into the upper ocean and then transits to depth where
it permanently increases the interior inventory by 60 Tmol
- 14 • Mt Pinatubo generated a temporary increase in the ocean carbon sink; a 0.29 ± 0.14 Pg
15 C yr^{-1} increase in 1992.
- 16
- 17

18 Abstract

19 Large volcanic eruptions drive significant climate perturbations through major anomalies in
20 radiative fluxes and the resulting widespread cooling of the surface and upper ocean. Recent
21 studies suggest that these eruptions also drive important variability in air-sea carbon and oxy-
22 gen fluxes. By simulating the Earth system using two initial-condition large ensembles, with
23 and without the aerosol forcing associated with the Mt. Pinatubo eruption in June 1991, we
24 isolate the impact of this event on ocean physical and biogeochemical properties. The Mt.
25 Pinatubo eruption generated significant anomalies in surface fluxes and the ocean interior in-
26 ventories of heat, oxygen, and carbon. Pinatubo-driven changes persist for multiple years in
27 the upper ocean and permanently modify the ocean's heat, oxygen, and carbon inventories.
28 Positive anomalies in oxygen concentrations emerge immediately post-eruption and penetrate
29 into the deep ocean. In contrast, carbon anomalies intensify in the upper ocean over several
30 years post-eruption, and are largely confined to the upper 150 m. In the tropics and northern
31 high latitudes, the change in oxygen is dominated by surface cooling and subsequent ven-
32 tilation to mid-depths, while the carbon anomaly is associated with solubility changes and
33 eruption-generated ENSO variability. Our results indicate that Pinatubo does not substan-
34 tially impact oxygen or carbon in the Southern Ocean; forced signals do not emerge from the
35 large internal variability in this region.

36 Plain Language Summary

37 The eruption of Pinatubo in June of 1991 produced sunlight-reflecting aerosols in the
38 upper atmosphere and led to a cooling of the planet for several years. While the global cool-
39 ing following the eruption is well documented, the impact of the eruption on the ocean oxy-
40 gen and carbon budgets has received comparably little attention. As the global ocean oxygen
41 concentration is declining in response to climate change, and as the ocean's continued stor-
42 age of anthropogenic carbon is critical for the climate system, it is of interest to quantify the
43 effect of the eruption on both oxygen and carbon in the global ocean. Here, we use an Earth
44 system model to simulate the historical evolution of the climate system both with and with-
45 out the Mt. Pinatubo eruption. By comparing the simulations, we are able to quantify the ef-
46 fect of the eruption on ocean properties. We find that the eruption led to cooler surface ocean
47 temperatures, and increases in the ocean oxygen and carbon concentrations that persisted for
48 many years. Our simulations can also be used to study other Earth system changes caused by
49 the eruption.

50 **1 Introduction**

51 As a result of anthropogenic activities, the global ocean is losing oxygen and gaining
 52 carbon. Observations indicate that the ocean's oxygen inventory has declined by about 2%
 53 in the 5 decades following 1960 as the upper ocean warms and stratifies [Ito *et al.*, 2017;
 54 Schmidtko *et al.*, 2017]. This oxygen loss has major consequences for nutrient cycling, com-
 55 pression of marine ecosystem habitats, and global fisheries [Keeling *et al.*, 2010; Gruber,
 56 2011; Deutsch *et al.*, 2015]. Since pre-industrial times, the ocean has absorbed ~170 Pg of
 57 anthropogenic carbon from the atmosphere [Canadell *et al.*, 2021], which is beneficial for
 58 the mitigation of anthropogenic warming, but harmful to some organisms through the related
 59 decline in pH, known as ocean acidification.

60 These long-term changes in ocean oxygen and carbon are superimposed on large in-
 61 terannual to multi-decadal variability, challenging the attribution of reported trends [Long
 62 *et al.*, 2016; McKinley *et al.*, 2016; Schlunegger *et al.*, 2020]. Due to their sensitivity to
 63 physical and biogeochemical processes, the oceanic oxygen concentrations and air-sea flux
 64 exhibit substantial variability across a range of timescales in observations and models [Ito
 65 *et al.*, 2010; McKinley *et al.*, 2003; Deutsch *et al.*, 2011; Eddebar *et al.*, 2017]. Modeling
 66 and observation-based studies suggest that both air-sea carbon dioxide flux and ocean car-
 67 bon concentrations exhibit variability on interannual to multi-decadal timescales [Resplandy
 68 *et al.*, 2015; DeVries *et al.*, 2017; Gruber *et al.*, 2019]. Many studies highlight internal cli-
 69 mate processes and modes of variability (e.g., El Niño - Southern Oscillation, North Atlantic
 70 Oscillation, Pacific Decadal Oscillation, Southern Annular Mode) as major drivers control-
 71 ling variations in the fluxes and inventories of global ocean oxygen and carbon [McKinley
 72 *et al.*, 2003, 2004; Lovenduski *et al.*, 2007; Deutsch *et al.*, 2011; Ito and Deutsch, 2013;
 73 Landschützer *et al.*, 2016; Eddebar *et al.*, 2017; McKinley *et al.*, 2017; Landschützer *et al.*,
 74 2019; Gruber *et al.*, 2019]. Others suggest an important role for externally driven climate
 75 perturbations (e.g., volcanic eruptions) in contributing to these variations [Frölicher *et al.*,
 76 2009; Frölicher *et al.*, 2011; Frölicher *et al.*, 2013; Eddebar *et al.*, 2019; McKinley *et al.*,
 77 2020]. It is critical that we develop a fundamental understanding of the drivers of past ocean
 78 oxygen and carbon variability so as to allow for clear interpretation of the observational
 79 record and also that we can more confidently predict future change.

80 Despite their well-known influence on global and regional climate [Marshall *et al.*,
 81 2022] and ocean heat uptake [Gupta and Marshall, 2018], the impact of volcanic eruptions

on ocean biogeochemistry is not well quantified. The explosive eruption of the Pinatubo strato-volcano in the Philippines on 15 June 1991 was the largest in the last 100 years. The volcanic release of sulfur dioxide and subsequent aerosols interaction in the stratosphere led to a substantial scattering of shortwave irradiance and a major reduction in solar heating at the sea surface, driving persistent global and regional changes in climate [Dutton and Christy, 1992; Marshall *et al.*, 2022]. The subsequent cooling effect from eruptions of this magnitude have the potential to cause a dramatic, though temporary, pause in global warming trends [Robock and Mao, 1995; Church *et al.*, 2005]. The eruption immediately preceded a boom in ocean observations occurring with the World Ocean Circulation Experiment (WOCE) and Joint Global Ocean Flux Study (JGOFS). Thus, it is possible the impacts from Pinatubo have been imprinted in these observations.

Past studies suggest that volcanic-induced climate perturbations can have a profound influence on the oceanic oxygen and carbon distributions and air-sea fluxes. Using a model ensemble, Frölicher *et al.* [2009] found that volcanic eruptions lead to an increase in interior ocean oxygen concentrations, with volcanic anomalies in oxygen gradually penetrating the top 500 m of the ocean and persisting for several years, but with considerable interannual to decadal variability. However, the small number of ensemble members (3 members) used in their study made regional attribution and process understanding of volcanic effects difficult due to confounding effects of internal (unforced) climate variability. A more recent modeling study leveraged the large number of ensemble members from the Community Earth System Model (CESM) and Geophysical Fluid Dynamics Laboratory model (GFDL) Large Ensembles (LENS) experiments to explore the volcanic effects from eruptions occurring since 1950 [Eddebar *et al.*, 2019]. They found that tropical eruptions generate strong and spatially decoupled ocean oxygen and carbon uptake, suggesting different processes at play throughout the ocean regions. The simulated oceanic oxygen uptake associated with the eruptions of Agung (1963), El Chichon (1982), and Pinatubo (1991) occurred primarily at mid and high latitudes and acted to reduce the magnitude of global ocean deoxygenation due to anthropogenic warming. This study also showcased strong carbon uptake at lower latitudes associated with an El Niño-like response to tropical eruptions in the tropical Pacific that is common across Earth system models [McGregor *et al.*, 2020]. While the large number of ensemble members substantially reduced the confounding influence of internal variability, the combined effect of various external forcings (anthropogenic greenhouse gases, industrial

114 aerosols, and volcanic aerosols) in this study challenges direct attribution and isolation of
 115 volcanic eruption effects on prolonged timescales.

116 In this study, we conduct numerical experiments that isolate the ocean's response to
 117 the volcanic forcing, so as to more clearly assess long-term deoxygenation trends and under-
 118 stand variations in carbon uptake and storage attributable to the Mt. Pinatubo eruption. We
 119 quantify the impacts of the Pinatubo eruption on ocean concentrations and air-sea fluxes of
 120 oxygen and carbon, and place them into context with anthropogenic forced changes and inter-
 121 nationally driven climate variability. While this paper is limited in scope to an introduction of the
 122 model experiments and the examination of oxygen and carbon impacts in the ocean, scien-
 123 tists throughout the community will find benefit from these runs for understanding the impact
 124 of Pinatubo throughout the climate system.

125 Here, the combined analysis of oxygen and carbon changes presents a unique and com-
 126plementary perspective on how ocean biogeochemistry and circulation respond to large scale
 127 radiative perturbations. Our tool for assessment of the impacts of Pinatubo is a set of large
 128 initial condition ensembles of the CESM Large Ensemble experiment, where each ensem-
 129 ble member has different phasing of internal climate variability. The first ensemble is forced
 130 with historical and projected future external forcing, while the second ensemble is forced
 131 identically with the sole exception that it excludes the aerosols due to the Pinatubo eruption.
 132 This experimental protocol permits a clean separation of the climate and biogeochemical im-
 133 pacts of the Pinatubo eruption on the Earth system.

134 First we will introduce the model setup experiments for this work. In section 3, we
 135 evaluate the global mean and spatial patterns of the difference between these two ensembles
 136 for SST, oxygen and carbon air-sea exchanges and inventories. We consider these as indica-
 137 tors of the impact of the eruption on the ocean's physical and biogeochemical state. In sec-
 138 tion 4, we discuss the mechanisms behind these changes, relationships to climate modes, and
 139 consider comparisons to observations and previous modeling work on the topic. Thoughts
 140 on the direction for future work are also included here. We conclude in section 5 with a sum-
 141 mary of our results.

142 2 Methods

143 To generate an initial-condition large ensemble, a climate model is run multiple times
 144 under identical forcing, but with very small perturbations in initial conditions. These per-

turbations evolve naturally and amplify rapidly, such that each ensemble member follows a unique climate trajectory through the phase space. The external forcing response, associated with the shared identical external forcing, is isolated in the mean across ensembles. Within the framework of NCAR's Community Earth System Model Large Ensemble (CESM-LE) effort [Kay *et al.*, 2015], we develop a new experiment with 29 members for 1990-2025 that explicitly excludes the forcing from Pinatubo (CESM-LE-NoPin) and isolates the externally forced response due to the volcanic eruption. The forced effect due to Pinatubo is quantified as the difference between the mean of 29 CESM-LE-NoPin ensemble members and the mean of the 29 CESM-LE members from which these were branched off. This forced effect is not directly observable in the real world. Instead, real world observations are akin to a single ensemble member that includes both the forced signal and internal variability [Deser *et al.*, 2012a,b]. As a coupled climate model, each ensemble member of CESM-LE develops its own phasing of internal variability that does not necessarily correspond with the phasing in the real world observations. The spread across the ensemble indicates the potential magnitude of the Earth system response to Pinatubo across multiple realizations of internal variability. Considering both the forced response and the internal spread, we evaluate the near-term and long-term interior ocean carbon and oxygen effects of Pinatubo, and connect these changes to surface flux patterns. Where appropriate, we place the forced changes and ensemble spread into context with observed changes in the ocean.

2.1 The Community Earth System Model

We use the CESM version 1 [CESM1; Hurrell *et al.*, 2013] to conduct our large ensemble simulations. CESM1 consists of atmosphere, ocean, land, and sea ice component models [Danabasoglu *et al.*, 2012; Lawrence *et al.*, 2012; Hunke and Lipscomb, 2008; Holland *et al.*, 2012]. The coupled atmospheric model is the Community Atmospheric Model version 5 (CAM5), integrated at nominal 1° horizontal resolution with 30 vertical levels [Hurrell *et al.*, 2013]. Volcanic radiative forcing is incorporated in the CESM LE using the forcing dataset of Ammann *et al.* [2003]. Stratospheric aerosol in CESM1-CAM5 is treated by prescribing a single, zonally averaged species. The prescription consists of a monthly mean mass distributed on a predefined meridional and vertical grid [Neely III *et al.*, 2016]. This aerosol mass is assumed to be comprised of 75% sulfuric acid and 25% water and to have a constant log-normal size distribution.

The ocean physical model, Parallel Ocean Program, version 2 [Smith *et al.*, 2010] has nominal 1° horizontal resolution and 60 vertical levels. Mesoscale eddy transport, diapycnal mixing, and mixed layer restratification by submesoscale eddies are parameterized with state-of-the-art approaches [Danabasoglu *et al.*, 2020]. The biogeochemical-ecosystem ocean model, known as the Biogeochemical Elemental Cycling (BEC) model, includes multi-nutrient co-limitation on phytoplankton growth and specific phytoplankton functional groups as well as full-depth ocean carbonate system thermodynamics, sea-to-air O₂ and CO₂ fluxes, and a dynamic iron cycle [Moore *et al.*, 2013]. The biogeochemical-ecosystem model compares favorably to observations, though there are some important biases, including weak Southern Ocean CO₂ uptake [Long *et al.*, 2013].

2.2 CESM No Pinatubo experiment (CESM-LE-NoPin)

The CESM-LE-NoPin setup is identical to the CESM-LE setup, but excludes the effect of the eruption by adjusting the volcanic aerosol mass mixing ratio within the model. Specifically, the volcanic aerosol mass mixing ratio values in CESM-LE-NoPin for January 1991 to December 1995 were replaced with values from January 1986 to December 1990 to simulate a time without impact from volcanic eruptions. Since Pinatubo was the dominant climatically important volcano during this period, we attribute the resulting climatic and ocean biogeochemical changes to Pinatubo. With this single change in the model setup, we are capturing effects attributable to the physical climate anomalies, however the methodology utilized in this model set up does not consider impacts from volcanic dust deposition on biomass production or other secondary feedbacks on the ocean from volcanic eruptions [Hamme *et al.*, 2010].

Conceptually, the CESM-LE-NoPin ensemble can be thought of as multiple realizations from a “control” climate that did not experience Pinatubo, while the original CESM-LE can be thought of as an “experiment” where each realization, or ensemble member, includes the eruption. We ran the 29 ensemble members of CESM-LE and CESM-LE-NoPin on the same supercomputer (NCAR Cheyenne) to avoid differences in output generated by machine and compiler changes; the original CESM-LE was run on NCAR’s Yellowstone machine.

204 **2.3 Statistical analysis**

205 We present Pinatubo-driven anomalies throughout the manuscript, where anomalies
 206 represent the difference between the CESM-LE and the CESM-LE-NoPin output. We quan-
 207 tify the forced impact of the eruption as the difference between the CESM-LE and CESM-
 208 LE-NoPin ensemble means (X). The internal variability is defined as the standard deviation
 209 (σ) across the ensemble members (CESM-LE minus CESM-LE-NoPin) at each time step.
 210 Analysis is conducted on monthly model output.

211 The forced impact of the eruption is statistically significant at the 95% confidence level
 212 [Deser *et al.*, 2012a] if its ratio of the ensemble mean difference (X) with the internal spread
 213 (σ) is greater than 2 divided by the square root of the degrees of freedom ($N-1$; here $N = 29$),

$$\frac{X}{\sigma} \geq \frac{2}{\sqrt{N-1}}. \quad (1)$$

214 When considering annual mean anomalies for the years following the eruption (Fig-
 215 ures 4-5), we use July as the first month of each year to ensure symmetry around the peak of
 216 ENSO. Consistent with previous work on the topic [Eddebar *et al.*, 2019], we refer to the
 217 12 months following the eruption as Year 0 [July 1991 -June 1992], and subsequent years as
 218 Year 1 [July 1992-June 1993], Year 2 [July 1993-June 1994], etc.

219 **3 Results**

220 Oxygen and carbon in the ocean are sensitive to a number of different physical pro-
 221 cesses in the climate system. In this section, we briefly describe the eruption-driven changes
 222 in ocean temperature, heat content, mixed layer depth, and circulation that are relevant for
 223 oxygen and carbon. We then perform a detailed investigation of the oxygen and carbon anom-
 224 alies driven by Pinatubo.

225 **3.1 Physical response to Pinatubo**

226 The eruption of Pinatubo in June of 1991 drives an immediate reduction in global
 227 mean sea surface temperature (SST) followed by a prolonged recovery (Figure 1a). The
 228 forced SST anomaly due to Pinatubo reaches a maximum of 0.18°C one year post-eruption,
 229 with a statistically significant cooling anomaly persisting for five years post eruption, despite
 230 an ensemble spread of $\pm 0.08^{\circ}\text{C}$ (Figure 1b). Below the sea surface, Pinatubo leads to a sub-

stantial heat loss, reaching a maximum of -3.5×10^{22} J across the entire water column by mid-1993, with most of this heat loss occurring in the upper 250 meters (Figure 2a,b, 3a). A globally averaged vertical profile Hovmöller plot of the difference of the two ensemble means (CESM-LE minus CESM-LE-NoPin) shows that significant cooling begins in 1992 for the upper ocean, with global-mean anomalies as large as 0.2°C penetrating down to 150m (Figure 3a). Smaller, but still significant, anomalies persist to depths below 1000m. Ocean heat content remains significantly altered by the eruption at the 95% confidence level through the year 2000 for the 250 m inventory and persists longer for full depth inventories (Figure 2b). Below 1000 m, the Pinatubo effect on heat content remains statistically significant for the duration of our experiments that end in 2024 (-2×10^{22} J, Figure S1), while the upper 250 m rebounds toward a heat content statistically indistinguishable from CESM-LE-NoPin after 2004 (Figure 2b). While there is some recovery in the two years following the maxima anomaly in OHC, the recovery stops quite abruptly in 1996 for all depths, and only modest changes are seen in the anomalies after that year, specifically at depths below 250m (Figure 2b). Our results show that Pinatubo causes a net heat loss that is not recovered even 3 decades after the eruption, consistent with previous modeling work [Frölicher *et al.*, 2011].

Spatial features of sea surface temperature anomalies show that Pinatubo-driven cooling is concentrated in the tropics in the year immediately following the eruption (Figure 4, left, Year 0). Cooling quickly spreads over much of the surface ocean by Year 1 (1992-93) with significant anomalies, given the spread of internal variability indicated by the model ensemble, throughout much of the Pacific basin (unstippled areas in Figure 4). In Year 1 there is also warming surface temperatures in the eastern equatorial Pacific, indicating the development of an El Niño event (Figure S4). In Year 2 (1993-94), this switches to a forced tendency to La Niña patterns in the equatorial Pacific, while northern hemisphere forced reductions in SST continue. In Year 3 (1994-95), the forced tendency to La Niña is the primary Pinatubo-driven cooling signal that persists. By Year 4 (1995-96), the forced surface cooling has largely dissipated, with internal variability masking any significant signal in the anomalies. Throughout the first 5 years post eruption (Year 0-4), no statistically significant cooling is simulated in the Southern Ocean. The Pacific sector of the Southern Ocean shows the strongest forced signal anomalies, although not emerging from the spread of internal variability, with warming during Year 0 and 1 followed by a cooling in subsequent years. These spatial maps indicate that the global-mean evolution of temperatures (Figure 3a) is initially

263 dominated by the Northern extratropics and then by a multi-year tendency to La Niña condi-
 264 tions in the equatorial Pacific.

265 Significant forced changes in maximum mixed layer depths (maxMLD) are spatially
 266 patchy, but do occur in extratropical locations important to upper and deep ocean ventila-
 267 tion (Figure 4, right). In the North Atlantic subpolar region across Years 0-4, there are some
 268 patches of significant forced maxMLD increases, particularly in the eastern gyre and in the
 269 Labrador and Irminger Seas. In the North Pacific, mode water regions experience significant
 270 forced increase in maxMLD in Year 0 and 1, and some forced decline in Year 4. Only weak
 271 forced change in maxMLD anomalies occur in scattered locations throughout the Southern
 272 Ocean.

273 **3.2 Oxygen and carbon response to Pinatubo**

274 The physical changes in temperature and circulation following Pinatubo are accompa-
 275 nied by pronounced changes in carbon and oxygen distributions and fluxes (Figure 1). The
 276 forced oxygen flux anomaly peaks at 42 Tmol yr^{-1} in 1992, with an ensemble spread (σ) of
 277 $\pm 31.5 \text{ Tmol yr}^{-1}$. The forced carbon flux anomaly reaches $0.29 \text{ Pg C yr}^{-1}$ in 1992, with an
 278 ensemble spread $\pm 0.14 \text{ Pg C yr}^{-1}$. The ensemble mean anomaly in O₂ and CO₂ flux is ro-
 279 bust at the 95% confidence level with the forced response of these fluxes persisting through
 280 1996 (Figure 1d,f). The global mean fluxes are large initially after the eruption due to the
 281 cooling of the surface ocean, but then the increased uptake weakens and rebounds to a sig-
 282 nificant forced reduction in the flux in years 1994-6 as cooling tapers off (Figure 1, left col-
 283 umn).

284 Oxygen and carbon inventory in the top 1000 m for both ensembles illustrate signifi-
 285 cant perturbations amid a backdrop of decreasing and increasing long-term trends, respec-
 286 tively (Figure 2c,e). The oxygen inventory time series reflects the global deoxygenation
 287 trend, and a clear divergence between the ensemble means of the CESM-LE and CESM-
 288 LE-NoPin experiments (Figure 2c). The anomalous oxygen uptake by the oceans immedi-
 289 ately following the eruption (Figure 1c,d) causes an increase in the O₂ content that is strong
 290 enough to temporarily counteract the effects of ocean deoxygenation. This pause in the de-
 291 oxygenation trend extends through 1995 before the decline resumes (Figure 2c).

292 There are significant Pinatubo-driven oxygen inventory anomalies for both the upper
 293 and deep ocean, with positive anomalies (increased oxygen content with the eruption) in the

upper ocean through 1998 (Figure 2d) and lagged changes for the full depth inventory extending for the entire 35 years of this experiment (Figure 2d, Figure S2). Post eruption, oxygen is immediately absorbed into the upper ocean and then transits to depth quickly where it permanently increases the interior inventory by 60 Tmol (Figure 2d). Globally averaged oxygen concentrations increase by as much as 1 mmol m^{-3} in the upper ocean following the eruption, reaching to depths of 250 m in early 1992 and subsequently spreading through the upper kilometer in 1994-1996 (Figure 3b). Anomalies then become insignificant for the global-averaged upper ocean above 250 m, but anomalies at depths greater than 250 m persist for the entire length of the simulation (Figure 3b, S3).

Pinatubo-driven anomalies in oxygen inventory exhibit large spatiotemporal variability across the ocean (Figure 5, left). The oxygen inventory of the upper 1000 m displays $\pm 2 \text{ mol m}^{-2}$ anomalies in the Northern hemisphere and the tropics in Years 1-3; anomalies in the Southern Ocean do not emerge until Years 3-4 and are concentrated in the Pacific sector (Figure 5, left). Positive anomalies, indicating greater depth-integrated oxygen due to Pinatubo, emerge first in the western boundary current regions of both the North Pacific and Atlantic basins in Year 1 post eruption, and traverse across the basin with time. In the North Atlantic, subpolar anomalies strengthen from Year 1 to Year 4, concurrent with cool SST anomalies and deeper mixed layer depths in that region (Figure 4). In the North Pacific, increased oxygen inventory is also linked with cool SST and deeper maxMLD anomalies (Figure 5, Figure 4). The positive anomalies in the North Pacific have only made it half way across the basin by Year 4, but the positive anomalies continue in that same trajectory in Years 5-9 (not shown). In these extratropical regions, Pinatubo-driven cooling, maxMLD deepening, and increased oxygen inventories are consistent with enhanced ventilation. The small regions exhibiting Pinatubo-driven maxMLD deepening correspond to critically important regions for upper ocean oxygenation [van Aken *et al.*, 2011; Deutsch *et al.*, 2006] and drive significant anomalies in the global mean oxygen inventory (Figure 2d, 3b).

Anomalous oxygen due to Pinatubo enters the ocean most quickly in the tropical Indian and Pacific, and quickly penetrates into and below the mixed layer in these basins (Figure 6, Figure S7-S8). The largest averaged anomalies are found in the North Pacific basin, exceeding 2 mmol m^{-3} for the regional-average anomaly in the upper ocean by two years post eruption (Figure 6). In all basins, Pinatubo-driven upper ocean oxygen anomalies exhibit seasonality, consistent with intermittent ventilation in wintertime (Figure 6). Anomalies in the North Pacific persist between 100-250m for over a decade. In the North Atlantic,

winter of Year 1 (1992-1993) experiences a ventilation anomaly that also causes anomalies greater than 2 mmol/m^3 between 100 and 250m. For multiple years post eruption, wintertime ventilation in the North Atlantic supplies anomalously high oxygen concentrations into the subsurface thermocline ((Figure 6), Figure S5) where oxygen eventually penetrates to depths below 500m (Figure S8). This signal also emerges through a strengthening of the Atlantic MOC during the late 1990s due to this increase in ventilation (Figure S10).

In contrast to the declining oxygen inventory due to ocean warming, Pinatubo-driven anomalies in air-sea CO_2 flux and DIC inventory occur against a background of increasing oceanic CO_2 uptake (Figure 1e) and a steadily increasing DIC inventory (Figure 2e) due to increasing atmospheric CO_2 concentrations prescribed in the modeled atmosphere. The carbon response is associated predominantly with preindustrial carbon, rather than anthropogenic (not shown); all results presented here are for the total carbon. The $0.29 \pm 0.14 \text{ Pg C yr}^{-1}$ increase in ocean uptake of carbon after the eruption (Figure 1e,f) leads to a modest, but statistically significant increase of the ocean DIC inventory of 0.53 Pg C in 1000m inventory by 1993 (Figure 2f) with anomalies most pronounced in the upper ocean (0.77 Pg C in the upper 250 m, Figure 2f). In contrast to oxygen inventories that increase with the depth of integration (Figure 2d), Pinatubo-driven anomalies in DIC inventory are largest in the upper ocean integrals and decrease with depth. Therefore the anomalies in the shallow depths and full integral become nearly consistent by 1998 (Figure 2f). Figure 3c clearly illustrates that the positive anomalies in global-mean DIC are concentrated in the upper 150 m of the ocean during years 1994-1997 (Figure 3c). The slower equilibration timescale for carbon helps to explain the slower DIC response relative to oxygen. Persistent significant anomalies of DIC due to Pinatubo are not detected at depths below 250 m in the global-mean profile, but there are short-lived forced oscillations between significant positive and negative anomalies of smaller magnitude.

Similar to oxygen, we find that Pinatubo-driven DIC anomalies exhibit spatial heterogeneity. For dissolved inorganic carbon inventory, we focus on the upper 250m (Figure 5) where the global mean profiles indicate the largest forced response (Figure 3c). Pinatubo's forced excitement of an El Niño event followed by a La Niña event (Figure S4) is expressed in the upper ocean DIC inventory; the Eastern (Western) Equatorial Pacific exhibits lower (elevated) DIC inventories one year post-eruption, while anomalously high DIC inventories can be found in the Eastern Equatorial Pacific during Years 2-3 post-eruption (Figure 5). In the extratropics, from Years 1-3, particularly in the North, there are also forced increases in

360 the upper ocean DIC content. This is consistent with increased solubility due to lower an-
 361 nual mean SST in these regions, particularly in Years 1 and 2 (Figure 4, left), that supports
 362 increased CO₂ fluxes across the air-sea interface (Figure S6).

363 The strongest positive forced anomalies in the upper ocean DIC inventory occur in the
 364 northern and tropical Pacific and tropical Indian, with some significant increase in the south
 365 Pacific as well (Figure 7, Figure S7). In the tropical Pacific, circulation anomalies associ-
 366 ated with ENSO modify the depth of the thermocline, generating opposite-signed anomalies
 367 with depth; the Pinatubo-driven El Niño event leads to decreased DIC in the upper 100 m,
 368 while the subsequent La Niña event produces $\sim >3 \text{ mmol m}^{-3}$ increases in upper ocean DIC
 369 concentrations (Figure 7). In the tropical Indian, thermocline oscillations also play a role in
 370 the inventory anomalies (Figure 7). In the Northern extratropics, upper ocean DIC anom-
 371 alies occur several years after the eruption (Figure 7). Unlike oxygen, the additional Pinatubo
 372 DIC is concentrated in the upper 100 m and generally does not penetrate to depth (Figure
 373 S9). The exception to this is in the tropical Atlantic which shows a positive DIC anomaly
 374 reaching down to below 250m by 1998 (Figure S9). Since our division of the regions is made
 375 at 30°N, this feature is most likely mode waters that are circulating in the upper subtropical
 376 gyre across the 30°N boundary. The positive anomaly persists throughout the length of the
 377 simulation at depths between 200 and 400m (Figure S9). In the South Pacific south of 30°S,
 378 there are modest positive forced anomalies in DIC above 200m in 1993-1996 (Year 2-4) but
 379 the other sectors of the Southern Ocean do not show a similar signal (Figure 7).

380 Despite clear forced signals in the upper ocean inventories of oxygen and carbon, forced
 381 signals in air-sea fluxes are difficult to discern with our model ensemble size (Figure S5-
 382 S6). Even with large signals in some regions, forced signals cannot be identified because
 383 of the large magnitude of internal variability in the fluxes (equation 1). Focusing on DJF-
 384 only fluxes (Figure S5-S6, right) to avoid seasonal cancellation of the signal, does allow for
 385 a forced signal to emerge in a few spots (eastern North Atlantic in Year 1 and 3), but on the
 386 whole does not allow a forced signal to be identified throughout much of the surface ocean.
 387 Inventories are integrated quantities that damp local internal variability, and allow forced sig-
 388 nals to more clearly emerge (Figure 1- 3).

389 Though the flux signals are not statistically identifiable as a forced response at the grid-
 390 scale, they do indicate a tendency for increased air-sea exchange of oxygen in North Pacific
 391 mode waters in Year 0 and 1 and in the North Atlantic subpolar gyre in Year 2-4 (Figure S5).

DJF anomalies are stronger than annual means in the north, consistent with ventilation being dominantly a wintertime phenomena. For carbon, the strongest annual mean anomalies occur in Year 1 (negative, increased uptake/less efflux with eruption) and in Year 3 and 4 (positive, reduced uptake/increase efflux with eruption) in the equatorial Pacific, consistent with ENSO variability (Figure S6). In DJF, there are some patches of significant flux anomalies at subtropical and subpolar latitudes that are mostly negative in Years 0-1 (indicating increased carbon uptake) and then are increasingly positive. These maps support the result that the ocean initially took up more carbon, but then the forced response involved a transition to a state with a reduced sink.

4 Discussion

4.1 Physical changes with Pinatubo

Our experiments with the CESM Large Ensemble allow precise separation of the physical impacts of Pinatubo and their spatio-temporal evolution in the presence of internal variability. Consistent with long-standing knowledge [Church *et al.*, 2005; Gleckler *et al.*, 2006a,b; Stenchikov *et al.*, 2009; Eddebbar *et al.*, 2019; Marshall *et al.*, 2022], we find that Pinatubo's eruption caused widespread global cooling, including spatially distinct reductions in SST, localized increases in maximum mixed layer depths and negative anomalies in upper ocean heat content. The forced surface cooling response, reaching a maximum of 0.18°C, is comparable to observations. NOAA's Optimum Interpolation Sea Surface Temperature (OISST) climate data record shows a global mean SST cooling of 0.12°C with a four year recovery time to return to pre-eruption global mean temperatures [Reynolds *et al.*, 2007].

The eruption of Pinatubo generates ENSO variability in CESM (Figure S4). A forced tendency to El Niño-like conditions emerges about one year after the eruption and is followed by La Niña-like conditions in subsequent years (Figure S4). Over half, or 15 members, of the CESM-LE members develop an El Niño event post-eruption 1992/3 (DJF), and all of those members develop a strong La Niña event in 1994/5 (DJF). In contrast, only 7 of the CESM-LE-NoPin ensemble members develop El Niños in 1992/3, with 6 of them developing a La Niña event in 1994/5. The significant ENSO response to the Pinatubo eruption in CESM-LE is consistent with other model experiments and paleoproxies that report the emergence of El Niño event in the year following a tropical eruption [Brad Adams *et al.*, 2003; Ohba *et al.*, 2013; Maher *et al.*, 2015; Stevenson *et al.*, 2017; Predybaylo *et al.*, 2017; Khodri

et al., 2017; Eddebar et al., 2019]. In the real world, the Pinatubo eruption occurred during a developing positive El Niño - Southern Oscillation (ENSO) index [NOAA, 2019]. The limitation of the real world is that it is difficult to cleanly discern the eruption-driven climatic signal from the phasing of internal climate variability and the background warming trend [Liu et al., 2018]. The impacts of ENSO preconditioning prior to a large eruption remain an outstanding challenge for the community studying impacts of volcanic eruptions on the climate system [Marshall et al., 2022; Swingedouw et al., 2017; Stevenson et al., 2017; Predabaylo et al., 2020; McGregor et al., 2020]. Though the extent and mechanisms driving this El Niño-like response in models are still debated [McGregor et al., 2020], the subsequent La Niña-like response to Pinatubo identified in CESM-LE has received little attention.

In contrast to the Pinatubo-driven ENSO response in CESM, the winter (DJF) North Atlantic Oscillation (NAO) index has a significant forced response to the eruption for only about one year during Year 3-4 (1994-1995), while the Southern Annular Mode (SAM) index does not show a significant forced response to the eruption at any time during the model run (Figure S4). This results are consistent with previous modeling studies considering strong volcanic eruptions impact on climate signals which found the tendency for NAO to persist in a positive phase over the first post-eruption decade, beginning in Year 3 post-eruption [Zanchettin et al., 2012]. Likewise for the SAM, McGraw et al. [2016] find that in years following major volcanic eruptions there is a tendency to a more positive median SAM index, however internal variability is large and ENSO state can impact this connection.

Additionally, our results show that Pinatubo forces an increase in the Atlantic Meridional Overturning Circulation (AMOC) by 1 Sv (4% of the mean), with individual ensemble members increasing by as much as 5 Sv (20% of the mean) (Figure S10). This is consistent with previous studies indicating that external forcing from volcanoes has an impact on the overturning circulation [Swingedouw et al., 2017; Fang et al., 2021]. The AMOC strengthening found in these CESM anomalies is larger and occurs earlier than that reported by Zanchettin et al. [2012]. In their last millennium ensemble results they find an AMOC intensification which culminates roughly one decade after the eruption with anomalies on the order of +0.5 Sv.

452 **4.2 Comparing Pinatubo impacts on carbon and oxygen**

453 Forced carbon and oxygen responses to Pinatubo have quite different spatial patterns
 454 (Figure 3,5, S5-S6), but the globally-averaged temporal evolution is reasonably similar. Oxy-
 455 gen is taken up at higher latitudes and deeper horizons than carbon which is primarily taken
 456 up at lower latitudes and further up the water column, in agreement with the findings of *Ed-*
 457 *debbar et al.* [2019]. Several aspects of the oxygen and carbon systems help to explain these
 458 features.

459 Oxygen has a much faster air-sea equilibration timescale than carbon, supporting larger
 460 and more immediate O₂ fluxes following the eruption. In addition, DIC concentrations in-
 461 crease downward while oxygen decreases with depth in the ocean; when cooling drives deeper
 462 mixing it brings up water low in O₂, but high in CO₂. Thus, ventilation promotes greater O₂
 463 fluxes, but dampens CO₂ fluxes, hence the larger O₂ uptake than carbon at higher latitudes.

464 Both carbon and oxygen fluxes experience an immediate forced global increase in
 465 ocean uptake and then a few years later, a rebound to a positive anomaly, or less uptake (Fig-
 466 ure 1c-f). For both gases, the air-sea gradient, $\Delta pX = pX^{atm} - pX^{ocean}$ (X = O₂ or CO₂), sets
 467 the magnitude of the flux. Any anomalous increase in uptake into the surface ocean raises
 468 pX^{*ocean*} and thus reduces the ΔX such that future fluxes will be damped [*Koch et al.*, 2009;
 469 *McKinley et al.*, 2020].

470 Together, these factors help to explain the larger amplitude anomalies in oxygen fluxes
 471 and the deeper penetration of oxygen inventory anomalies. When the surface ocean cools and
 472 low oxygen waters are delivered to the surface, oxygen can rapidly be exchanged across the
 473 air-sea interface and injected into the deep ocean [*Körtzinger et al.*, 2004; *Atamanchuk et al.*,
 474 2020] (Figure 3,6). The window to the surface ocean then closes and the oxygen anomalies
 475 are transported at depth (Figure 3).

476 In contrast, the immediate cooling with Pinatubo primarily increases the carbon carry-
 477 ing capacity by increasing carbon solubility at the surface. Air-sea carbon exchange slowly
 478 adds DIC to the ocean and seasonal mixing and mode water formation spreads this anomaly
 479 in the upper 150m. In the tropics, fluxes are modulated by the ENSO cycle, leading to re-
 480 duced outgassing with the initial post-eruption El Niño, and then additional outgassing with
 481 the subsequent La Niña event (Figure S6-S7). The accumulation of DIC in the upper ocean
 482 in the first years after the eruption is concentrated in the North Pacific, Indian, and Southern

483 Ocean (Figure S7). This accumulation acts to create a back pressure on fluxes in Years 2-3
 484 after the eruption (Figure 1e,f, 5, S6).

485 **4.3 Pinatubo impact on oxygen fluxes and inventories**

486 Previous model experiments [*Frölicher et al.*, 2009; *Eddebar et al.*, 2019] suggest
 487 a potentially important role for volcanic eruptions in interrupting ocean deoxygenation and
 488 modulating the pronounced interannual-to-decadal variability of the observed ocean oxygen
 489 content. The global mean oxygen anomalies forced by Pinatubo, which are isolated in our
 490 study, are considerable given current trends measured in the world's ocean. Models predict
 491 a decline in the global ocean dissolved oxygen inventory of 1-7% by the year 2100 [*Keel-*
 492 *ing et al.*, 2010] and estimate that 55 Tmol per year was lost in the 1990s [*Schmidtko et al.*,
 493 2017]. Our model results indicate that the eruption of Pinatubo led to maximum increase in
 494 interior oxygen of about 100 Tmol in the top 1000m over the 4 years following the eruption
 495 (Figure 2, 3), more than offsetting the expected deoxygenation for the first half of 1990s and
 496 leading to a net increase in the oxygen inventory of about 60 Tmol by the end of the simula-
 497 tion.

498 Another interesting feature of our results is that oxygen anomalies are decoupled in
 499 depth from temperature changes in CESM, suggesting processes such as changes in trans-
 500 port or biogeochemical rates as drivers of oxygen uptake in addition to the solubility effects,
 501 as previously suggested by [*Eddebar et al.*, 2019]. For example, temperature anomalies
 502 are pronounced in upper 0-100 m, while O₂ anomalies are intensified in the 50-200 m depth
 503 range (Figure 3). Oxygen changes are also generally more pronounced at depth below 250m
 504 (Figure 2d, Figure S8), which may offer new insights on the response of ocean circulation to
 505 volcanic eruptions. The intensification of the AMOC (Figure S10) suggests an increase in
 506 the advective supply of oxygen to depth as a result of volcanic eruption in the Atlantic basin.
 507 Pronounced cooling and a deepened mixed layer at mid and high latitudes likely lead to in-
 508 tensified oxygen uptake and subduction of newly ventilated waters to depth.

509 **4.4 Mechanisms of air-sea CO₂ flux anomalies with Pinatubo**

510 *McKinley et al.* [2020] used a simple box model forced with atmospheric pCO₂ and
 511 global-mean upper ocean heat content anomalies associated with tropical volcanos to pro-
 512 pose a mechanistic explanation for globally integrated air-sea CO₂ flux anomalies since the

513 1980s. The box model closely replicates ($r>0.9$) the signals found in ensembles of ocean
 514 hindcast models and observation-based pCO_2 products. Based on this evidence, *McKinley*
 515 *et al.* [2020] were the first to propose a significant role for external forcing from Pinatubo in
 516 the variability of the ocean carbon sink in the 1990s.

517 Here, with CESM-LE, we find a significant forced anomaly of $0.29 \text{ Pg C yr}^{-1}$ in the
 518 1992 globally-integrated air-sea CO_2 flux forced by Pinatubo in CESM-LE; and individ-
 519 ual members of the ensemble have flux anomalies greater than 0.5 Pg C yr^{-1} (Figure 1e,f).
 520 CESM-LE also reveals significant spatial structure in the carbon flux and DIC inventory
 521 response to the eruption of Pinatubo—the ocean’s carbon response to Pinatubo is far from
 522 globally uniform (Figure 5,7, S6). In the subtropics and the northern high latitudes, the up-
 523 per ocean absorbs more carbon, particularly in the subtropics, while ENSO dominates the
 524 tropical response (Figure 5, 7). This heterogeneous spatial response is not at all captured in
 525 the box model, yet the box model’s CO_2 flux anomaly of 0.5 Pg C yr^{-1} is within a factor of
 526 two of the CESM-LE forced response. CESM-LE also indicates a similar forced reduction
 527 in the ocean carbon sink in 1994-1995 as in the box model. This feature is consistent with
 528 more DIC being held in the upper ocean (Figure 5) where it can raise surface ocean pCO_2
 529 and damp the flux (Figure S6) [*McKinley et al.*, 2020].

530 The evolution of the global-mean ocean heat content (OHC) and global-mean DIC
 531 profile (Figure 3) demonstrates the global-mean relationship between upper ocean cooling
 532 and DIC content that the box model successfully mimics. The forced change in OHC due to
 533 Pinatubo ($-3.5 \times 10^{22} \text{ J}$) is within the range estimated from observations and other modeling
 534 studies [*Church et al.*, 2005; *Gleckler et al.*, 2006a, 2016; *Stenchikov et al.*, 2009; *Eddebar*
 535 *et al.*, 2019; *DeVries*, 2022]. The OHC anomaly in the 200 m deep box model of *McKinley*
 536 *et al.* [2020] is within a factor of two ($-5.5 \times 10^{22} \text{ J}$). As in the box model, the globally aver-
 537 aged behavior of CESM-LE is for the negative OHC anomalies to enhance solubility and
 538 allow for enhanced air-sea fluxes to persist for long enough (several years) such that addi-
 539 tional carbon can be absorbed in the upper ocean (Figure 3). These CESM-LE experiments
 540 demonstrate both this global-mean forced response and allow for deeper understanding of the
 541 spatially variable mechanisms forced by Pinatubo.

542 Another study looking at the external forcing of the Pinatubo eruption on the climate
 543 system found a cooling of upper ocean (0-300m) ocean heat content and a subsequent re-
 544 covery to near zero OHC anomaly by 1996 [*DeVries*, 2022]. However, the models used by

545 *DeVries* [2022] utilize only historical SST to represent Pinatubo's external forcing in a steady
546 circulation ocean model. Since these SST anomalies impacted only the top model layer of 10
547 m depth, the resulting globally-integrated OHC anomaly with Pinatubo (-1×10^{22} J) was sub-
548 stantially smaller than most observational studies [*Church et al.*, 2005; *DeVries*, 2022] and
549 more than 3 times smaller than the forced response estimated here with CESM-LE. There-
550 fore their resulting small externally forced air-sea CO₂ flux response is consistent with the
551 underestimation of globally-integrated upper ocean cooling and the lack of ENSO response
552 or ventilation changes in a model with steady circulation.

553 CESM-LE demonstrates a clear CO₂ flux anomaly due to Pinatubo in the global in-
554 tegral (Figure 1e,f). But at the local scale, air-sea flux anomalies rarely have a statistically
555 significant forced response (Figure S6). This is because the large internal variability in sur-
556 face fluxes obscures the forced signal. This finding is directly comparable to the finding that
557 the air-sea CO₂ flux response to COVID-19 emissions reductions is not detectable at the lo-
558 cal scale [*Lovenduski et al.*, 2021]. Large internal variability presents a particular challenge
559 to the potential for local flux observations to directly identify climatic signals and argues for
560 continued integration of data into observation-based products from which large-scale signals
561 can be identified [*Fay and McKinley*, 2021; *Fay et al.*, 2021].

562 CESM-LE indicates that the regional centers for CO₂ flux anomalies due to Pinatubo
563 are primarily in the Northern hemisphere and the tropics, but not in the Southern Ocean (Fig-
564 ure S6). This contrasts to observation-based products that suggest large amplitude decadal
565 variability in Southern Ocean CO₂ fluxes [*Landschützer et al.*, 2015; *Hauck et al.*, 2020;
566 *Bennington et al.*, 2012]. Other mechanisms may be responsible for observed large ampli-
567 tude Southern Ocean decadal variability [*Gruber et al.*, 2019]. Alternatively, in-situ sam-
568 pling [*Bakker et al.*, 2016] in the Southern Ocean may have been too sparse to allow for ac-
569 curate reconstructions [*Gloege et al.*, 2021]. With respect to global mechanisms, CESM-LE
570 indicates that the more vigorous overturning of the 1990s, identified by *DeVries et al.* [2017]
571 as a potential mechanism for ocean carbon sink variability, may have been externally forced
572 by Pinatubo. Better quantifying the magnitude and mechanisms of CO₂ flux decadal vari-
573 ability globally and in the Southern Ocean is an important focal point for current ocean car-
574 bon research.

575 **4.5 Future Work**

576 With this analysis, we have only just begun to explore all the insights available regarding
 577 the impact of the Pinatubo eruption on the ocean and its biogeochemistry. There is much
 578 more to be done in terms of understanding the full extent of Pinatubo's impact on ocean
 579 physics and biogeochemistry at global, regional, and local scales.

580 Integrated column inventories and globally integrated fluxes clearly demonstrate the
 581 impact of Pinatubo on ocean oxygen and carbon, but locally, significant forced changes in
 582 air-sea fluxes are difficult to identify (Figure S6). Because of the magnitude of internal vari-
 583 ability at the surface, future work could expand the number of ensemble members to pinpoint
 584 forced changes in surface fluxes.

585 We highlight here that the Pinatubo effects on ocean biogeochemistry explored in this
 586 modeling experiment include the climate impacts of volcanic aerosols on ocean biogeochem-
 587 istry but do not simulate direct biogeochemical changes associated with increased micronu-
 588 trient deposition from volcanic ash. Observational studies of smaller eruptions suggest vol-
 589 canic ash deposition may significantly influence carbon cycling through fertilizing plankton
 590 growth at regional scales [Hamme *et al.*, 2010; Langman *et al.*, 2010]. The direct bioge-
 591 ochemical contribution of atmospheric deposition of micronutrients by volcanic ash may have
 592 additional and complex effects on carbon and oxygen distributions and inventories. These
 593 effects are outside the scope of this work, but are worth examining in follow on experiments.

594 CESM is just one of many Earth system models that have previously generated large
 595 ensembles [Deser *et al.*, 2020]. All models are imperfect representations of the real Earth -
 596 for example, this version of CESM underestimates Southern Ocean CO₂ uptake [Long *et al.*,
 597 2013] and we do not know if this bias has a role in the small Southern Ocean impacts from
 598 Pinatubo that we find here. It would be of great value to have other modeling centers conduct
 599 large ensembles without Pinatubo so that different estimates of forced responses and repre-
 600 sentation of volcanic aerosol forcings could be compared.

601 We are currently using the CESM ensembles to investigate the impact of the Pinatubo
 602 eruption on hydrographic observations of ocean biogeochemistry [Olivarez, H.C., Loven-
 603 duski, N.S., Eddebar, Y.A., Fay, A.R., Levy, M., Long, M.C., and McKinley, G.A., *The Im-*
 604 *pact of the Pinatubo Climate Perturbation on Global Ocean Carbon and Biogeochemistry,*
 605 *in preparation for Global Biogeochemical Cycles*]. The bulk of ocean biogeochemical ob-

606 servations that anchor long-term trends were collected in the years following the Pinatubo
607 eruption through the World Ocean Circulation Experiment / Joint Global Ocean Flux Study
608 (WOCE / JGOFS) [Boyer, 2018].

609 Comprehensive model output is available for scientists to investigate other components
610 of the Earth system, such as the atmosphere, sea ice and cryosphere.

611 5 Conclusions

612 With two initial-condition large ensembles, we have isolated the impacts of the 1991
613 eruption of Mt. Pinatubo on ocean physical and biogeochemical properties. Pinatubo forced
614 the ocean to cool to a peak of 0.18°C at the surface and to lose $3.5 \times 10^{22} \text{ J}$ of heat. Pinatubo
615 forced an El Niño event one year after the eruption, and then La Niña for the two subsequent
616 years. Upper ocean ventilation increased in key regions, allowing for the penetration of oxy-
617 gen anomalies to depth. These simulations indicate that the long-term effect of Pinatubo on
618 the ocean heat budget was a loss of $2 \times 10^{22} \text{ J}$ that persists for multiple decade.

619 Associated with these physical changes, the ocean absorbed oxygen and carbon, with
620 peak globally integrated forced flux anomalies in 1992 of $42 \text{ Tmol O}_2 \text{ yr}^{-1}$ and 0.29 Pg C
621 yr^{-1} , respectively. In the tropics and northern high latitudes, the eruption's impact on oxygen
622 is dominated by surface cooling and subsequent ventilation to mid-depths, while the carbon
623 anomaly is associated with solubility changes and eruption-generated ENSO variability. In-
624 creased inventories of both gases are found mostly in the tropics and Northern hemisphere,
625 but are very limited in the Southern Ocean. Oxygen anomalies penetrate to the deep ocean,
626 while carbon anomalies remain concentrated in the upper 150 m. For both, full-depth inven-
627 tories are permanently altered.

628 Acknowledgments

629 The authors acknowledge high-performance computing support from Cheyenne
630 (<https://doi.org/10.5065/D6RX99HX>) provided by NCAR's Computational and Information
631 Systems Laboratory, sponsored by the National Science Foundation (NSF). This material is
632 based upon work supported by the National Center for Atmospheric Research, which is a ma-
633 jor facility sponsored by the National Science Foundation under Cooperative Agreement No.
634 1852977. We are grateful for support from the National Science Foundation (OCE-1948624,

635 OCE-1948664, OCE-1948728, AGS-2019625, OCE 1948599). We acknowledge the previ-
 636 ous work done by the CESM Large Ensemble Community Project.

637 Open Research: The CESM source code is freely available at <http://www2.cesm.ucar.edu>.
 638 The model outputs described in this paper can be accessed at www.earthsystemgrid.org.

639 References

- 640 Ammann, C. M., G. A. Meehl, W. M. Washington, and C. S. Zender (2003), A monthly and
 641 latitudinally varying volcanic forcing dataset in simulations of 20th century climate, *Geo-*
 642 *physical Research Letters*, 30(12), doi:<https://doi.org/10.1029/2003GL016875>.
- 643 Atamanchuk, D., J. Koelling, U. Send, and D. W. R. Wallace (2020), Rapid transfer of oxy-
 644 gen to the deep ocean mediated by bubbles, *Nature Geoscience*, 13(3), 232–237, doi:
 645 10.1038/s41561-020-0532-2.
- 646 Bakker, D. C. E., B. Pfeil, C. S. Landa, N. Metzl, K. M. O'Brien, A. Olsen, K. Smith,
 647 C. Cosca, S. Harasawa, S. D. Jones, S.-I. Nakaoka, Y. Nojiri, U. Schuster, T. Stein-
 648 hoff, C. Sweeney, T. Takahashi, B. Tilbrook, C. Wada, R. Wanninkhof, S. R. Alin, C. F.
 649 Balestrini, L. Barbero, N. R. Bates, A. A. Bianchi, F. Bonou, J. Boutin, Y. Bozec, E. F.
 650 Burger, W.-J. Cai, R. D. Castle, L. Chen, M. Chierici, K. Currie, W. Evans, C. Feather-
 651 stone, R. A. Feely, A. Fransson, C. Goyet, N. Greenwood, L. Gregor, S. Hankin, N. J.
 652 Hardman-Mountford, J. Harley, J. Hauck, M. Hoppema, M. P. Humphreys, C. W. Hunt,
 653 B. Huss, J. S. P. Ibánhez, T. Johannessen, R. Keeling, V. Kitidis, A. Kötzinger, A. Kozyr,
 654 E. Krasakopoulou, A. Kuwata, P. Landschützer, S. K. Lauvset, N. Lefèvre, C. Lo Monaco,
 655 A. Manke, J. T. Mathis, L. Merlivat, F. J. Millero, P. M. S. Monteiro, D. R. Munro, A. Mu-
 656 rata, T. Newberger, A. M. Omar, T. Ono, K. Paterson, D. Pearce, D. Pierrot, L. L. Rob-
 657 bins, S. Saito, J. Salisbury, R. Schlitzer, B. Schneider, R. Schweitzer, R. Sieger, I. Skjel-
 658 van, K. F. Sullivan, S. C. Sutherland, A. J. Sutton, K. Tadokoro, M. Telszewski, M. Tuma,
 659 S. M. A. C. van Heuven, D. Vandemark, B. Ward, A. J. Watson, and S. Xu (2016), A
 660 multi-decade record of high-quality $f\text{CO}_2$ data in version 3 of the Surface Ocean CO_2
 661 Atlas (SOCAT), *Earth Syst. Sci. Data*, 8(2), 383–413, doi:10.5194/essd-8-383-2016.
- 662 Bennington, V., G. A. McKinley, N. R. Urban, and C. P. McDonald (2012), Can spatial het-
 663 erogeneity explain the perceived imbalance in Lake Superior's carbon budget? A model
 664 study, *J. Geophys. Res. Biogeosci.*, 117(G3), doi:10.1029/2011JG001895.
- 665 Boyer, O. B. C. C. H. G. A. G. R. L. A. M. C. P. J. R. D. S. I. S. K. W. M. Z., T.P. (2018),
 666 *World Ocean Database 2018*, A. V. Mishonov, Technical Editor, NOAA Atlas NESDIS

- 667 87.
- 668 Brad Adams, J., M. E. Mann, and C. M. Ammann (2003), Proxy evidence for an el niño-like
669 response to volcanic forcing, *Nature*, 426(6964), 274–278, doi:10.1038/nature02101.
- 670 Canadell, J. G., P. M. S. Monteiro, M. H. Costa, L. C. da Cunha, P. M. Cox, A. V. Eliseev,
671 S. Henson, M. Ishii, S. Jaccard, C. Koven, A. Lohila, P. K. Patra, S. Piao, J. Rogelj,
672 S. Syampungani, S. Zaehle, and K. Zickfeld (2021), Global Carbon and other Biogeo-
673 chemical Cycles and Feedbacks, *Climate Change 2021: The Physical Science Basis.*
674 *Contribution of Working Group I to the Sixth Assessment Report of the Intergovernmen-*
675 *tal Panel on Climate Change [Masson-Delmotte, V., P. Zhai, A. Pirani, S. L. Connors,*
676 *C. Péan, S. Berger, N. Caud, Y. Chen, L. Goldfarb, M. I. Gomis, M. Huang, K. Leitzell,*
677 *E. Lonnoy, J.B.R. Matthews, T. K. Maycock, T. Waterfield, O. Yelekçi, R. Yu and B. Zhou*
678 *(eds.)].*
- 679 Church, J. A., N. J. White, and J. M. Arblaster (2005), Significant decadal-scale impact of
680 volcanic eruptions on sea level and ocean heat content, *Nature*, 438(7064), 74–77.
- 681 Danabasoglu, G., S. C. Bates, B. P. Briegleb, S. R. Jayne, M. Jochum, W. G. Large, S. Pea-
682 cock, and S. G. Yeager (2012), The CCSM4 Ocean Component, *J. Climate*, 25(5), 1361–
683 1389.
- 684 Danabasoglu, G., J. F. Lamarque, J. Bacmeister, D. A. Bailey, A. K. DuVivier, J. Edwards,
685 L. K. Emmons, J. Fasullo, R. Garcia, A. Gettelman, C. Hannay, M. M. Holland, W. G.
686 Large, P. H. Lauritzen, D. M. Lawrence, J. T. M. Lenaerts, K. Lindsay, W. H. Lipscomb,
687 M. J. Mills, R. Neale, K. W. Oleson, B. Otto-Bliesner, A. S. Phillips, W. Sacks, S. Tilmes,
688 L. van Kampenhout, M. Vertenstein, A. Bertini, J. Dennis, C. Deser, C. Fischer, B. Fox-
689 Kemper, J. E. Kay, D. Kinnison, P. J. Kushner, V. E. Larson, M. C. Long, S. Mickel-
690 son, J. K. Moore, E. Nienhouse, L. Polvani, P. J. Rasch, and W. G. Strand (2020), The
691 Community Earth System Model version 2 (CESM2), *J. Adv. Model. Earth Syst.*, 12(2),
692 e2019MS001,916, doi:10.1029/2019MS001916.
- 693 Deser, C., A. Phillips, V. Bourdette, and H. Teng (2012a), Uncertainty in climate change pro-
694 jections: the role of internal variability, *Clim. Dynam.*, 38(3-4), 527–546, doi:10.1007/
695 s00382-010-0977-x.
- 696 Deser, C., R. Knutti, S. Solomon, and A. S. Phillips (2012b), Communication of the role of
697 natural variability in future North American climate, *Nature Clim. Change*, 2(11), 775–
698 779.

- 699 Deser, C., F. Lehner, K. B. Rodgers, T. Ault, T. L. Delworth, P. N. DiNezio, A. Fiore,
700 C. Frankignoul, J. C. Fyfe, D. E. Horton, J. E. Kay, R. Knutti, N. S. Lovenduski,
701 J. Marotzke, K. A. McKinnon, S. Minobe, J. Randerson, J. A. Screen, I. R. Simpson, and
702 M. Ting (2020), Insights from Earth system model initial-condition large ensembles and
703 future prospects, *Nature Clim. Change*, 10(4), 277–286, doi:10.1038/s41558-020-0731-2.
- 704 Deutsch, C., S. Emerson, and L. Thompson (2006), Physical-biological interactions in north
705 pacific oxygen variability, *Journal of Geophysical Research: Oceans*, 111(C9), doi:<https://doi.org/10.1029/2005JC003179>.
- 706 Deutsch, C., H. Brix, T. Ito, H. Frenzel, and L. Thompson (2011), Climate-forced variability
707 of ocean hypoxia, *Science*, 333(6040), 336–339, doi:10.1126/science.1202422.
- 708 Deutsch, C., A. Ferrel, B. Seibel, H.-O. Pörtner, and R. B. Huey (2015), Climate change
709 tightens a metabolic constraint on marine habitats, *Science*, 348(6239), 1132–1135, doi:
710 10.1126/science.aaa1605.
- 711 DeVries, T. (2022), Atmospheric CO_2 and sea surface temperature variability cannot ex-
712 plain recent decadal variability of the ocean CO_2 sink, *Geophysical Research Letters*,
713 49(7), e2021GL096,018, doi:<https://doi.org/10.1029/2021GL096018>, e2021GL096018
714 2021GL096018.
- 715 DeVries, T., M. Holzer, and F. Primeau (2017), Recent increase in oceanic carbon uptake
716 driven by weaker upper-ocean overturning, *Nature*, 542(7640), 215–218.
- 717 Dutton, E. G., and J. R. Christy (1992), Solar radiative forcing at selected locations and ev-
718 idence for global lower tropospheric cooling following the eruptions of el chichón and
719 pinatubo, *Geophysical Research Letters*, 19(23), 2313–2316, doi:<https://doi.org/10.1029/92GL02495>.
- 720 Eddebar, Y. A., M. C. Long, L. Resplandy, C. Rödenbeck, K. B. Rodgers, M. Manizza,
721 and R. F. Keeling (2017), Impacts of enso on air-sea oxygen exchange: Observations and
722 mechanisms, *Global Biogeochemical Cycles*, 31(5), 901–921, doi:<https://doi.org/10.1002/2017GB005630>.
- 723 Eddebar, Y. A., K. B. Rodgers, M. C. Long, A. C. Subramanian, S.-P. Xie, and R. F. Keel-
724 ing (2019), El Niño-like physical and biogeochemical ocean response to tropical erup-
725 tions, *J. Climate*, 32(9), 2627–2649, doi:10.1175/JCLI-D-18-0458.1.
- 726 Fang, S.-W., M. Khodri, C. Timmreck, D. Zanchettin, and J. Jungclaus (2021), Disentan-
727 gling internal and external contributions to atlantic multidecadal variability over the
728 past millennium, *Geophysical Research Letters*, 48(23), e2021GL095,990, doi:<https://doi.org/10.1029/2021GL095990>.
- 729
- 730
- 731

- 732 //doi.org/10.1029/2021GL095990, e2021GL095990 2021GL095990.
- 733 Fay, A. R., and G. A. McKinley (2021), Observed regional fluxes to constrain modeled esti-
734 mates of the ocean carbon sink, *Geophysical Research Letters*, 48(20), e2021GL095,325,
735 doi:<https://doi.org/10.1029/2021GL095325>, e2021GL095325 2021GL095325.
- 736 Fay, A. R., L. Gregor, P. Landschützer, G. A. McKinley, N. Gruber, M. Gehlen, Y. Iida, G. G.
737 Laruelle, C. Rödenbeck, A. Roobaert, and J. Zeng (2021), Seafux: harmonization of air-
738 sea CO_2 fluxes from surface pCO_2 data products using a standardized approach, *Earth Sys-*
739 *tem Science Data*, 13(10), 4693–4710, doi:10.5194/essd-13-4693-2021.
- 740 Frölicher, T. L., F. Joos, G.-K. Plattner, M. Steinacher, and S. C. Doney (2009), Natural vari-
741 ability and anthropogenic trends in oceanic oxygen in a coupled carbon cycle–climate
742 model ensemble, *Global Biogeochem. Cycles*, 23(1), doi:10.1029/2008GB003316.
- 743 Frölicher, T. L., F. Joos, and C. C. Raible (2011), Sensitivity of atmospheric CO_2 and cli-
744 mate to explosive volcanic eruptions, *Biogeosciences*, 8(8), 2317–2339, doi:10.5194/
745 bg-8-2317-2011.
- 746 Frölicher, T. L., F. Joos, C. C. Raible, and J. L. Sarmiento (2013), Atmospheric CO_2 re-
747 sponse to volcanic eruptions: The role of ENSO, season, and variability, *Global Bio-*
748 *geochem. Cycles*, 27(1), 239–251, doi:<https://doi.org/10.1002/gbc.20028>.
- 749 Gleckler, P. J., K. AchutaRao, J. M. Gregory, B. D. Santer, K. E. Taylor, and T. M. L. Wigley
750 (2006a), Krakatoa lives: The effect of volcanic eruptions on ocean heat content and
751 thermal expansion, *Geophysical Research Letters*, 33(17), doi:<https://doi.org/10.1029/2006GL026771>.
- 752 Gleckler, P. J., T. M. L. Wigley, B. D. Santer, J. M. Gregory, K. AchutaRao, and K. E. Taylor
753 (2006b), Krakatoa's signature persists in the ocean, *Nature*, 439(7077), 675–675, doi:10.
754 1038/439675a.
- 755 Gleckler, P. J., P. J. Durack, R. J. Stouffer, G. C. Johnson, and C. E. Forest (2016), Industrial-
756 era global ocean heat uptake doubles in recent decades, *Nature Climate Change*, 6(4),
757 394–398, doi:10.1038/nclimate2915.
- 758 Gloege, L., G. A. McKinley, P. Landschützer, A. R. Fay, T. L. Frölicher, J. C. Fyfe, T. Ily-
759 ina, S. Jones, N. S. Lovenduski, K. B. Rodgers, S. Schlunegger, and Y. Takano (2021),
760 Quantifying errors in observationally based estimates of ocean carbon sink variabil-
761 ity, *Global Biogeochem. Cycles*, 35(4), e2020GB006,788, doi:<https://doi.org/10.1029/2020GB006788>.

- 764 Gruber, N. (2011), Warming up, turning sour, losing breath: Ocean biogeochemistry under
765 global change, *Phil. Trans. R. Soc. A.*, 369(1943), 1980–1996.
- 766 Gruber, N., D. Clement, B. R. Carter, R. A. Feely, S. van Heuven, M. Hoppema, M. Ishii,
767 R. M. Key, A. Kozyr, S. K. Lauvset, C. Lo Monaco, J. T. Mathis, A. Murata, A. Olsen,
768 F. F. Perez, C. L. Sabine, T. Tanhua, and R. Wanninkhof (2019), The oceanic sink for
769 anthropogenic co₂ from 1994 to 2007, *Science*, 363(6432), 1193, doi:
770 10.1126/science.aau5153.
- 771 Gupta, M., and J. Marshall (2018), The climate response to multiple volcanic eruptions me-
772 diated by ocean heat uptake: Damping processes and accumulation potential, *Journal of*
773 *Climate*, 31(21), 8669 – 8687, doi:10.1175/JCLI-D-17-0703.1.
- 774 Hamme, R. C., P. W. Webley, W. R. Crawford, F. A. Whitney, M. D. DeGrandpre, S. R.
775 Emerson, C. C. Eriksen, K. E. Giesbrecht, J. F. R. Gower, M. T. Kavanaugh, M. A. Peña,
776 C. L. Sabine, S. D. Batten, L. A. Coogan, D. S. Grundle, and D. Lockwood (2010), Vol-
777 canic ash fuels anomalous plankton bloom in subarctic northeast pacific, *Geophysical Re-*
778 *search Letters*, 37(19), doi:<https://doi.org/10.1029/2010GL044629>.
- 779 Hauck, J., M. Zeising, C. Le Quéré, N. Gruber, D. C. E. Bakker, L. Bopp, T. T. T.
780 Chau, Ö. Gürses, T. Ilyina, P. Landschützer, A. Lenton, L. Resplandy, C. Rödenbeck,
781 J. Schwinger, and R. Séférian (2020), Consistency and challenges in the ocean carbon sink
782 estimate for the Global Carbon Budget, *Front. Mar. Sci.*, 7, 852, doi:10.3389/fmars.2020.
783 571720.
- 784 Holland, M. M., D. A. Bailey, B. P. Briegleb, B. Light, and E. Hunke (2012), Improved sea
785 ice shortwave radiation physics in CCSM4: The impact of melt ponds and aerosols on
786 Arctic sea ice, *J. Climate*, 25(5), 1413–1430, doi:10.1175/JCLI-D-11-00078.1.
- 787 Hunke, E. C., and W. H. Lipscomb (2008), CICE: the Los Alamos sea ice model user's man-
788 ual, version 4, *Los Alamos Natl. Lab. Tech. Report, LA-CC-06-012*.
- 789 Hurrell, J. W., M. M. Holland, P. R. Gent, S. Ghan, J. E. Kay, P. J. Kushner, J. F. Lamar-
790 que, W. G. Large, D. Lawrence, K. Lindsay, W. H. Lipscomb, M. C. Long, N. Mahowald,
791 D. R. Marsh, R. B. Neale, P. Rasch, S. Vavrus, M. Vertenstein, D. Bader, W. D. Collins,
792 J. J. Hack, J. Kiehl, and S. Marshall (2013), The Community Earth System Model: A
793 Framework for Collaborative Research, *B. Am. Meteorol. Soc.*, 94(9), 1339–1360, doi:
794 10.1175/BAMS-D-12-00121.1.
- 795 Ito, T., and C. Deutsch (2013), Variability of the oxygen minimum zone in the tropical north
796 pacific during the late twentieth century, *Global Biogeochemical Cycles*, 27(4), 1119–

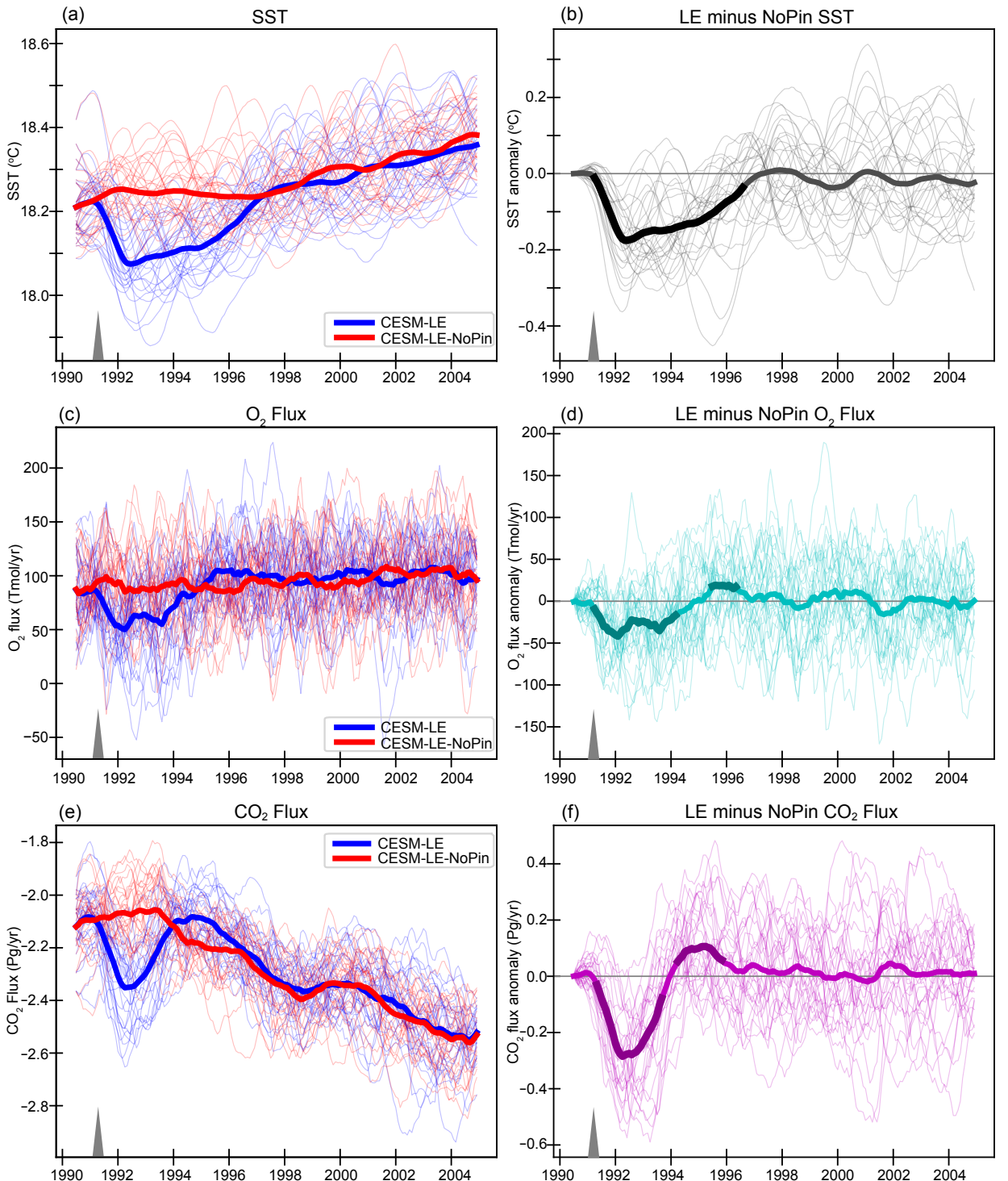
- 797 1128, doi:<https://doi.org/10.1002/2013GB004567>.
- 798 Ito, T., M. Woloszyn, and M. Mazloff (2010), Anthropogenic carbon dioxide transport in the
799 Southern Ocean driven by Ekman flow, *Nature*, 463(7277), 80–83.
- 800 Ito, T., S. Minobe, M. C. Long, and C. Deutsch (2017), Upper ocean O_2 trends: 1958–
801 2015, *Geophysical Research Letters*, 44(9), 4214–4223, doi:<https://doi.org/10.1002/2017GL073613>.
- 802 Kay, J. E., C. Deser, A. Phillips, A. Mai, C. Hannay, G. Strand, J. M. Arblaster, S. C. Bates,
803 G. Danabasoglu, J. Edwards, M. Holland, P. Kushner, J. F. Lamarque, D. Lawrence,
804 K. Lindsay, A. Middleton, E. Munoz, R. Neale, K. Oleson, L. Polvani, and M. Vertenstein
805 (2015), The Community Earth System Model (CESM) Large Ensemble project: A com-
806 munity resource for studying climate change in the presence of internal climate variability,
807 *B. Am. Meteorol. Soc.*, 96(8), 1333–1349, doi:10.1175/BAMS-D-13-00255.1.
- 808 Keeling, R. F., A. Körtzinger, and N. Gruber (2010), Ocean Deoxygenation in a Warming
809 World, *Annu. Rev. Mar. Sci.*, 2(1), 199–229, doi:10.1146/annurev.marine.010908.163855.
- 810 Khodri, M., T. Izumo, J. Vialard, S. Janicot, C. Cassou, M. Lengaigne, J. Mignot,
811 G. Gastineau, E. Guilyardi, N. Lebas, A. Robock, and M. J. McPhaden (2017), Tropical
812 explosive volcanic eruptions can trigger el niño by cooling tropical africa, *Nature Commu-*
813 *nications*, 8(1), 778, doi:10.1038/s41467-017-00755-6.
- 814 Koch, J., G. A. McKinley, V. Bennington, and D. Ullman (2009), Do hurricanes cause sig-
815 nificant interannual variability in the air-sea CO_2 flux of the subtropical North Atlantic?,
816 *Geophys. Res. Lett.*, 36(7), doi:10.1029/2009GL037553.
- 817 Körtzinger, A., J. Schimanski, U. Send, and D. Wallace (2004), The Ocean Takes a Deep
818 Breath, *Science*, 306(5700), 1337, doi:10.1126/science.1102557.
- 819 Landschützer, P., N. Gruber, F. A. Haumann, C. Rödenbeck, D. C. E. Bakker, S. van Heuven,
820 M. Hoppema, N. Metzl, C. Sweeney, T. Takahashi, B. Tilbrook, and R. Wanninkhof
821 (2015), The reinvigoration of the Southern Ocean carbon sink, *Science*, 349(6253), 1221–
822 1224.
- 823 Landschützer, P., N. Gruber, and D. C. E. Bakker (2016), Decadal variations and trends of
824 the global ocean carbon sink, *Global Biogeochem. Cycles*, 30(10), 1396–1417, doi:10.
825 1002/2015GB005359, 2015GB005359.
- 826 Landschützer, P., T. Ilyina, and N. S. Lovenduski (2019), Detecting regional modes of vari-
827 ability in observation-based surface ocean pCO_2 , *Geophys. Res. Lett.*, 46(5), 2670–2679,
828 doi:10.1029/2018GL081756.

- 830 Langman, O., P. Hanson, S. Carpenter, and Y. Hu (2010), Control of dissolved oxygen in
831 northern temperate lakes over scales ranging from minutes to days, *Aquatic Biology*, 9(2),
832 193–202.
- 833 Lawrence, D. M., K. W. Oleson, M. G. Flanner, C. G. Fletcher, P. J. Lawrence, S. Levis,
834 S. C. Swenson, and G. B. Bonan (2012), The CCSM4 land simulation, 1850–2005: As-
835 sessment of surface climate and new capabilities, *J. Climate*, 25(7), 2240–2260, doi:
836 10.1175/JCLI-D-11-00103.1.
- 837 Liu, F., C. Xing, L. Sun, B. Wang, D. Chen, and J. Liu (2018), How do tropical, northern
838 hemispheric, and southern hemispheric volcanic eruptions affect enso under different
839 initial ocean conditions?, *Geophysical Research Letters*, 45(23), 13,041–13,049, doi:
840 <https://doi.org/10.1029/2018GL080315>.
- 841 Long, M. C., K. Lindsay, S. Peacock, J. K. Moore, and S. C. Doney (2013), Twentieth-
842 Century Oceanic Carbon Uptake and Storage in CESM1(BGC), *J. Climate*, 26(18), 6775–
843 6800, doi:10.1175/JCLI-D-12-00184.1.
- 844 Long, M. C., C. Deutsch, and T. Ito (2016), Finding forced trends in oceanic oxygen, *Global*
845 *Biogeochem. Cycles*, 30(2), 381–397, doi:10.1002/2015GB005310, 2015GB005310.
- 846 Lovenduski, N. S., N. Gruber, S. C. Doney, and I. D. Lima (2007), Enhanced CO₂ outgassing
847 in the Southern Ocean from a positive phase of the Southern Annular Mode, *Global Bio-*
848 *geochem. Cycles*, 21(2), GB2026, doi:10.1029/2006GB002900.
- 849 Lovenduski, N. S., N. C. Swart, A. J. Sutton, J. C. Fyfe, G. A. McKinley, C. Sabine, and
850 N. L. Williams (2021), The ocean carbon response to COVID-related emissions re-
851 ductions, *Geophys. Res. Lett.*, 48(6), e2020GL092,263, doi:<https://doi.org/10.1029/2020GL092263>.
- 853 Maher, N., S. McGregor, M. H. England, and A. S. Gupta (2015), Effects of volcanism on
854 tropical variability, *Geophysical Research Letters*, 42(14), 6024–6033, doi:<https://doi.org/10.1002/2015GL064751>.
- 856 Marshall, L. R., E. C. Maters, A. Schmidt, C. Timmreck, A. Robock, and M. Toohey (2022),
857 Volcanic effects on climate: recent advances and future avenues, *Bulletin of Volcanology*,
858 84(5), 54, doi:10.1007/s00445-022-01559-3.
- 859 McGraw, M. C., E. A. Barnes, and C. Deser (2016), Reconciling the observed and modeled
860 southern hemisphere circulation response to volcanic eruptions, *Geophysical Research*
861 *Letters*, 43(13), 7259–7266, doi:<https://doi.org/10.1002/2016GL069835>.

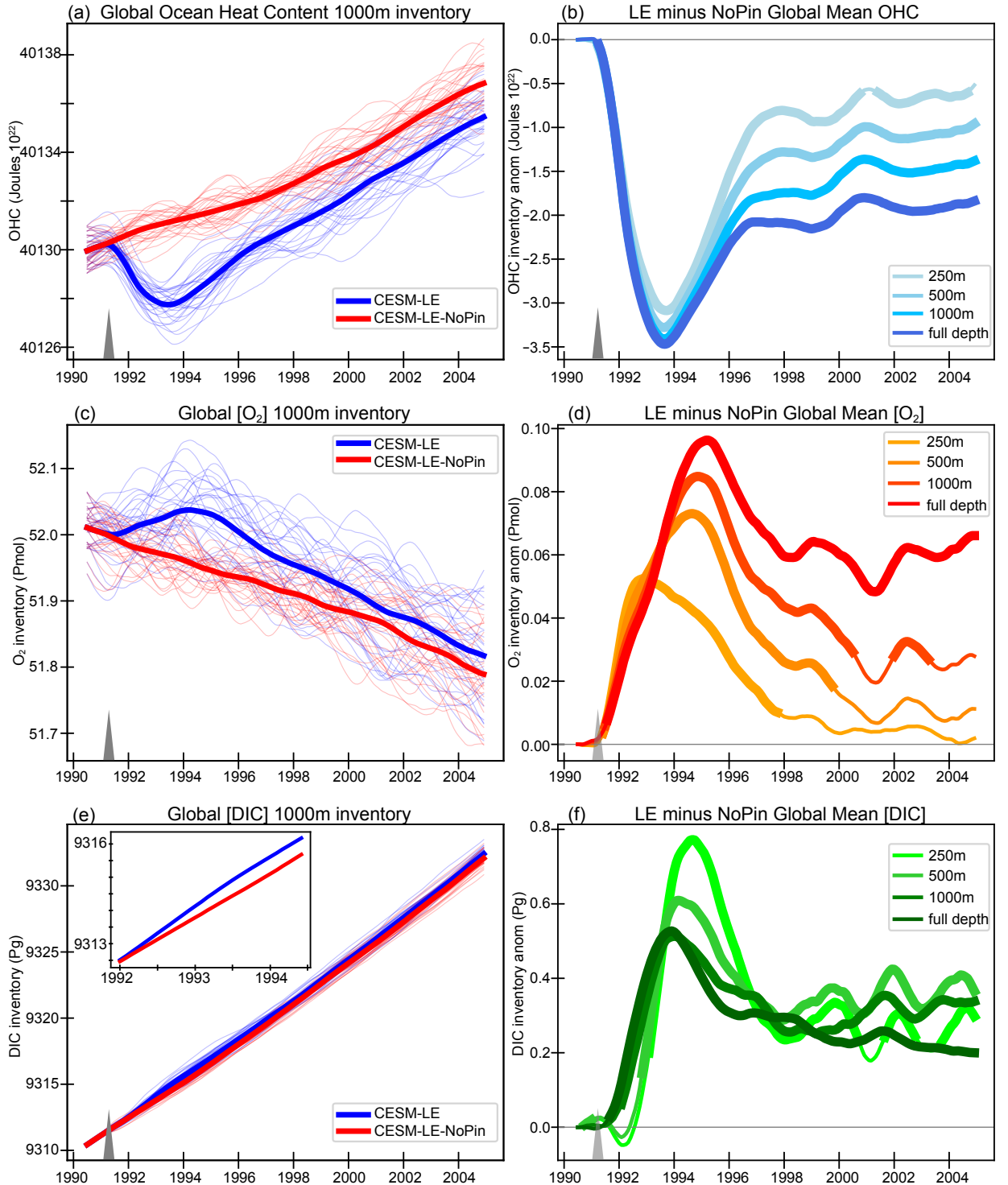
- 862 McGregor, S., M. Khodri, N. Maher, M. Ohba, F. S. R. Pausata, and S. Stevenson (2020),
863 *The Effect of Strong Volcanic Eruptions on ENSO*, chap. 12, pp. 267–287, American Geo-
864 physical Union (AGU), doi:<https://doi.org/10.1002/9781119548164.ch12>.
- 865 McKinley, G. A., M. J. Follows, J. Marshall, and S.-M. Fan (2003), Interannual variability of
866 air-sea O₂ fluxes and the determination of CO₂ sinks using atmospheric O₂/N₂, *Geophysical*
867 *Research Letters*, 30(3), doi:<https://doi.org/10.1029/2002GL016044>.
- 868 McKinley, G. A., M. J. Follows, and J. Marshall (2004), Mechanisms of air-sea CO₂ flux
869 variability in the equatorial Pacific and the North Atlantic, *Global Biogeochem. Cycles*,
870 18(2), C07S06, doi:[10.1029/2003GB002179](https://doi.org/10.1029/2003GB002179).
- 871 McKinley, G. A., D. J. Pilcher, A. R. Fay, K. Lindsay, M. C. Long, and N. S. Lovenduski
872 (2016), Timescales for detection of trends in the ocean carbon sink, *Nature*, 530(7591),
873 469–472.
- 874 McKinley, G. A., A. R. Fay, N. S. Lovenduski, and D. J. Pilcher (2017), Natural variability
875 and anthropogenic trends in the ocean carbon sink, *Annu. Rev. Mar. Sci.*, 9(1), 125–150,
876 doi:[10.1146/annurev-marine-010816-060529](https://doi.org/10.1146/annurev-marine-010816-060529).
- 877 McKinley, G. A., A. R. Fay, Y. A. Eddebar, L. Gloege, and N. S. Lovenduski (2020), External
878 forcing explains recent decadal variability of the ocean carbon sink, *AGU Advances*,
879 1(2), e2019AV000149, doi:[10.1029/2019AV000149](https://doi.org/10.1029/2019AV000149).
- 880 Moore, J. K., K. Lindsay, S. C. Doney, M. C. Long, and K. Misumi (2013), Marine ecosystem
881 dynamics and biogeochemical cycling in the Community Earth System Model
882 [CESM1(BGC)]: Comparison of the 1990s with the 2090s under the RCP4.5 and RCP8.5
883 scenarios, *J. Climate*, 26(23), 9291–9312, doi:[10.1175/JCLI-D-12-00566.1](https://doi.org/10.1175/JCLI-D-12-00566.1).
- 884 Neely III, R. R., A. J. Conley, F. Vitt, and J.-F. Lamarque (2016), A consistent prescription
885 of stratospheric aerosol for both radiation and chemistry in the community earth sys-
886 tem model (cesm1), *Geoscientific Model Development*, 9(7), 2459–2470, doi:[10.5194/gmd-9-2459-2016](https://doi.org/10.5194/gmd-9-2459-2016).
- 888 NOAA (2019), National Oceanic and Atmospheric Administration.
- 889 Ohba, M., H. Shiogama, T. Yokohata, and M. Watanabe (2013), Impact of strong tropical
890 volcanic eruptions on enso simulated in a coupled gcm, *Journal of Climate*, 26(14), 5169
891 – 5182, doi:[10.1175/JCLI-D-12-00471.1](https://doi.org/10.1175/JCLI-D-12-00471.1).
- 892 Predybaylo, E., G. L. Stenchikov, A. T. Wittenberg, and F. Zeng (2017), Impacts of a
893 pinatubo-size volcanic eruption on enso, *Journal of Geophysical Research: Atmospheres*,
894 122(2), 925–947, doi:<https://doi.org/10.1002/2016JD025796>.

- 895 Predybaylo, E., G. Stenchikov, A. T. Wittenberg, and S. Osipov (2020), El niño/southern
896 oscillation response to low-latitude volcanic eruptions depends on ocean pre-conditions
897 and eruption timing, *Communications Earth & Environment*, 1(1), 12, doi:10.1038/
898 s43247-020-0013-y.
- 899 Resplandy, L., R. Séférian, and L. Bopp (2015), Natural variability of CO₂ and O₂ fluxes:
900 What can we learn from centuries-long climate models simulations?, *J. Geophys. Res.
901 Oceans*, 120(1), 384–404, doi:10.1002/2014JC010463.
- 902 Reynolds, R. W., T. M. Smith, C. Liu, D. B. Chelton, K. S. Casey, and M. G. Schlax (2007),
903 Daily high-resolution-blended analyses for sea surface temperature, *Journal of Climate*,
904 20(22), 5473 – 5496, doi:10.1175/2007JCLI1824.1.
- 905 Robock, A., and J. Mao (1995), The volcanic signal in surface temperature observations,
906 *Journal of Climate*, 8(5), 1086 – 1103, doi:10.1175/1520-0442(1995)008<1086:TVSIST>
907 2.0.CO;2.
- 908 Schlunegger, S., K. B. Rodgers, J. L. Sarmiento, T. Ilyina, J. P. Dunne, Y. Takano, J. R.
909 Christian, M. C. Long, T. L. Frölicher, R. Slater, and F. Lehner (2020), Time of Emer-
910 gence and Large Ensemble intercomparison for ocean biogeochemical trends, *Global Bio-
911 geochem. Cycles*, 34(8), e2019GB006,453, doi:<https://doi.org/10.1029/2019GB006453>.
- 912 Schmidtko, S., L. Stramma, and M. Visbeck (2017), Decline in global oceanic oxygen con-
913 tent during the past five decades, *Nature*, 542(7641), 335–339, doi:10.1038/nature21399.
- 914 Smith, R., P. Jones, B. Briegleb, F. Bryan, G. Danabasoglu, J. Dennis, J. Dukowicz, C. Eden,
915 B. Fox-Kemper, P. Gent, M. Hecht, S. Jayne, M. Jochum, W. Large, K. Lindsay, M. Mal-
916 trud, N. Norton, S. Peacock, M. Vertenstein, and S. Yeager (2010), *The Parallel Ocean
917 Program (POP) Reference Manual*, Los Alamos National Laboratory Tech. Rep. LAUR-
918 10-01853, Los Alamos, NM.
- 919 Stenchikov, G., T. L. Delworth, V. Ramaswamy, R. J. Stouffer, A. Wittenberg, and F. Zeng
920 (2009), Volcanic signals in oceans, *Journal of Geophysical Research: Atmospheres*,
921 114(D16), doi:<https://doi.org/10.1029/2008JD011673>.
- 922 Stevenson, S., J. T. Fasullo, B. L. Otto-Bliesner, R. A. Tomas, and C. Gao (2017), Role of
923 eruption season in reconciling model and proxy responses to tropical volcanism, *Pro-
924 ceedings of the National Academy of Sciences*, 114(8), 1822–1826, doi:10.1073/pnas.
925 1612505114.
- 926 Swingedouw, D., J. Mignot, P. Ortega, M. Khodri, M. Menegoz, C. Cassou, and V. Hanquiez
927 (2017), Impact of explosive volcanic eruptions on the main climate variability modes,

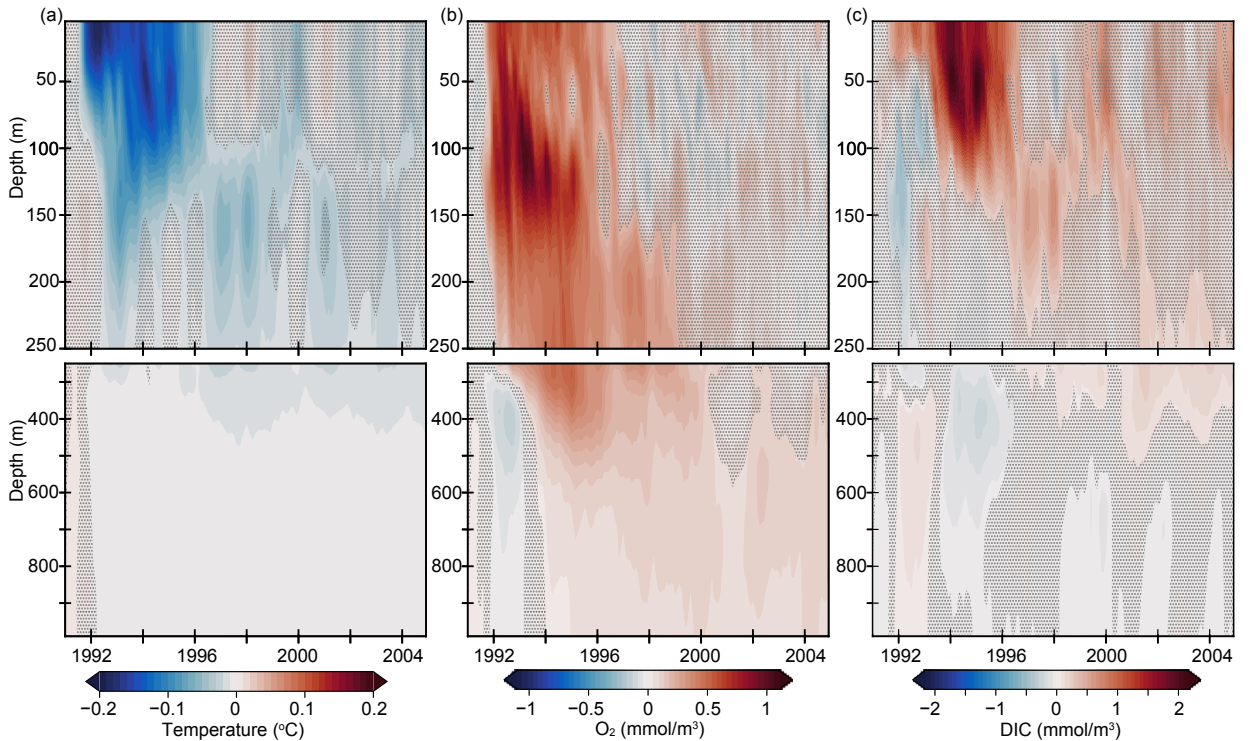
- 928 *Global and Planetary Change*, 150, 24–45, doi:<https://doi.org/10.1016/j.gloplacha.2017.01.006>.
- 929
- 930 van Aken, H. M., M. F. de Jong, and I. Yashayaev (2011), Decadal and multi-decadal vari-
- 931 ability of Labrador Sea Water in the north-western North Atlantic Ocean derived from
- 932 tracer distributions: Heat budget, ventilation, and advection, *Deep-Sea Res. I*, 58(5), 505 –
- 933 523, doi:<https://doi.org/10.1016/j.dsr.2011.02.008>.
- 934 Zanchettin, D., C. Timmreck, H. F. Graf, A. Rubino, S. Lorenz, K. Lohmann, K. Krüger, and
- 935 J. H. Jungclaus (2012), Bi-decadal variability excited in the coupled ocean–atmosphere
- 936 system by strong tropical volcanic eruptions, *Climate Dynamics*, 39(1), 419–444, doi:[10.1007/s00382-011-1167-1](https://doi.org/10.1007/s00382-011-1167-1).
- 937



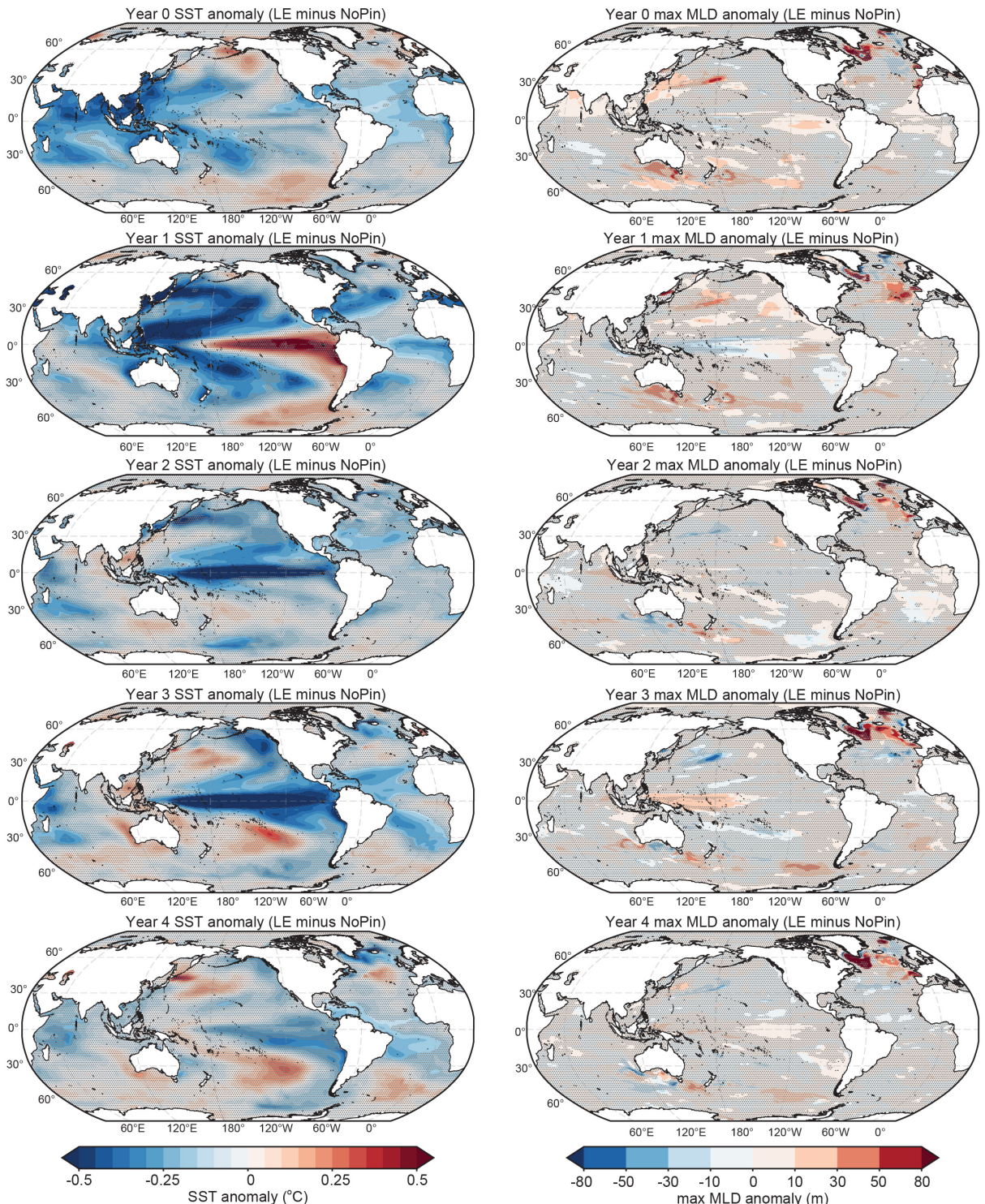
938 **Figure 1.** Left column: CESM-LE (blue) and CESM-LE-NoPin (red) individual members (thin lines) and
 939 ensemble mean (thick line) time series for global mean SST (top, degC), Oxygen flux (middle, Tmol/yr), and
 940 CO₂ Flux (bottom, Pg/yr) for 1990-2004. Right column: CESM-LE minus CESM-LE-NoPin difference for
 941 each variable with thicker line indicating significant difference between the two ensembles at 2σ [Deser *et al.*,
 942 2012a]. Time series are seasonally detrended and smoothed with a 12-month running mean. Gray triangles
 943 mark timing of eruption. Full time series through 2025 available in Figure S1.



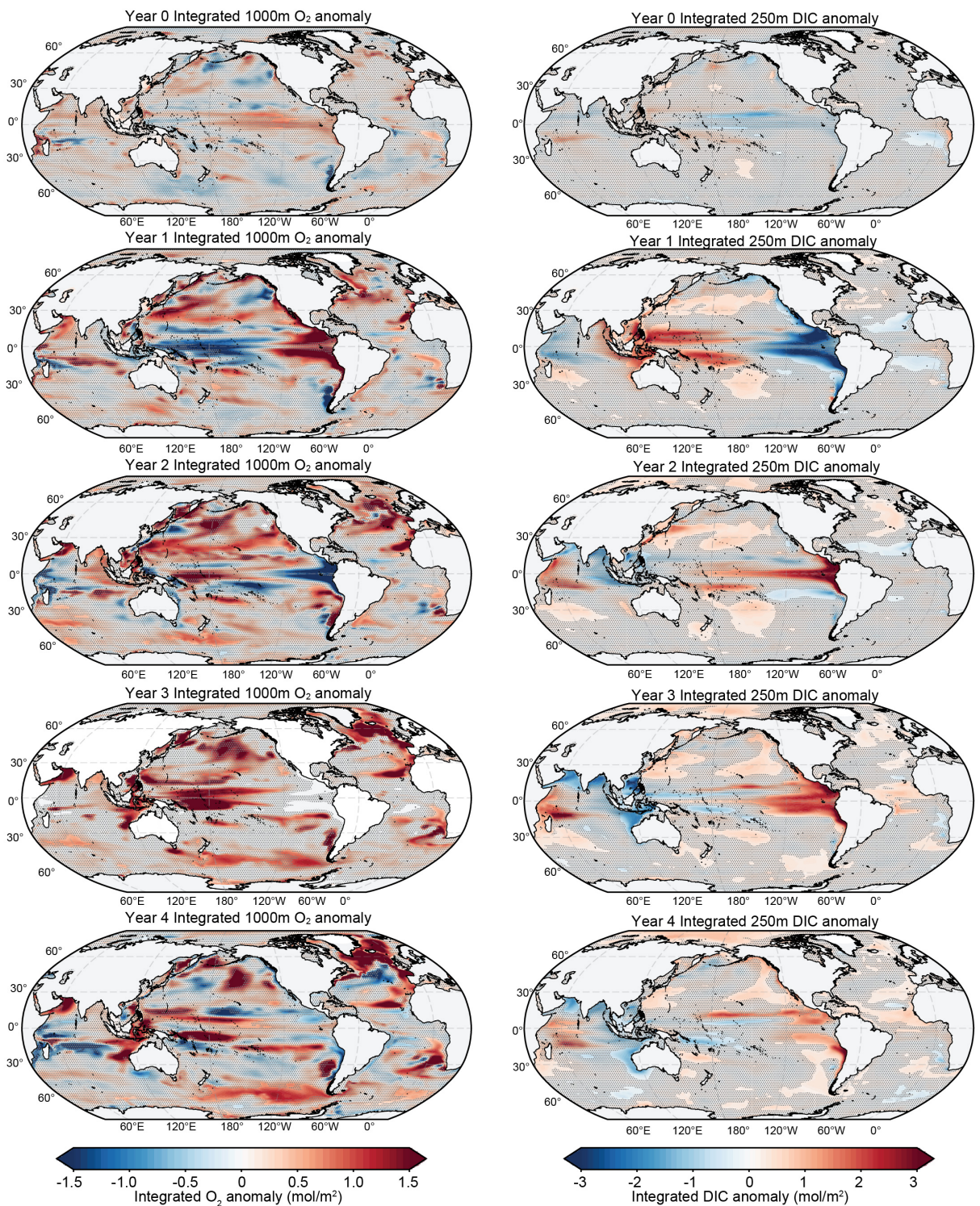
944 **Figure 2.** Left column: CESM-LE (blue) and CESM-LE-NoPin (red) individual members (thin lines)
945 and ensemble mean (thick line) time series for global mean Ocean Heat Content (top, Joules 10^{22}), Oxygen
946 inventory (middle, Pmol), and Dissolved Inorganic Carbon inventory (bottom, Pg) for top 1000m. Inset on
947 DIC inventory (bottom, left) shows a zoomed in ensemble mean time series for 1992-1995 to highlight the
948 difference post eruption. Right column: CESM-LE minus CESM-LE-NoPin inventory difference for each
949 variable with thicker line indicating significant difference between two ensembles at 2σ [Deser et al., 2012a].
-33-
950 Inventory plots include lines for depths 250m, 500m, 1000m and full depth. Time series are seasonally de-
951 trended, smoothed with a 12-month running mean. Gray triangle marks timing of eruption. Full time series
952 through 2025 available in Figure S2.



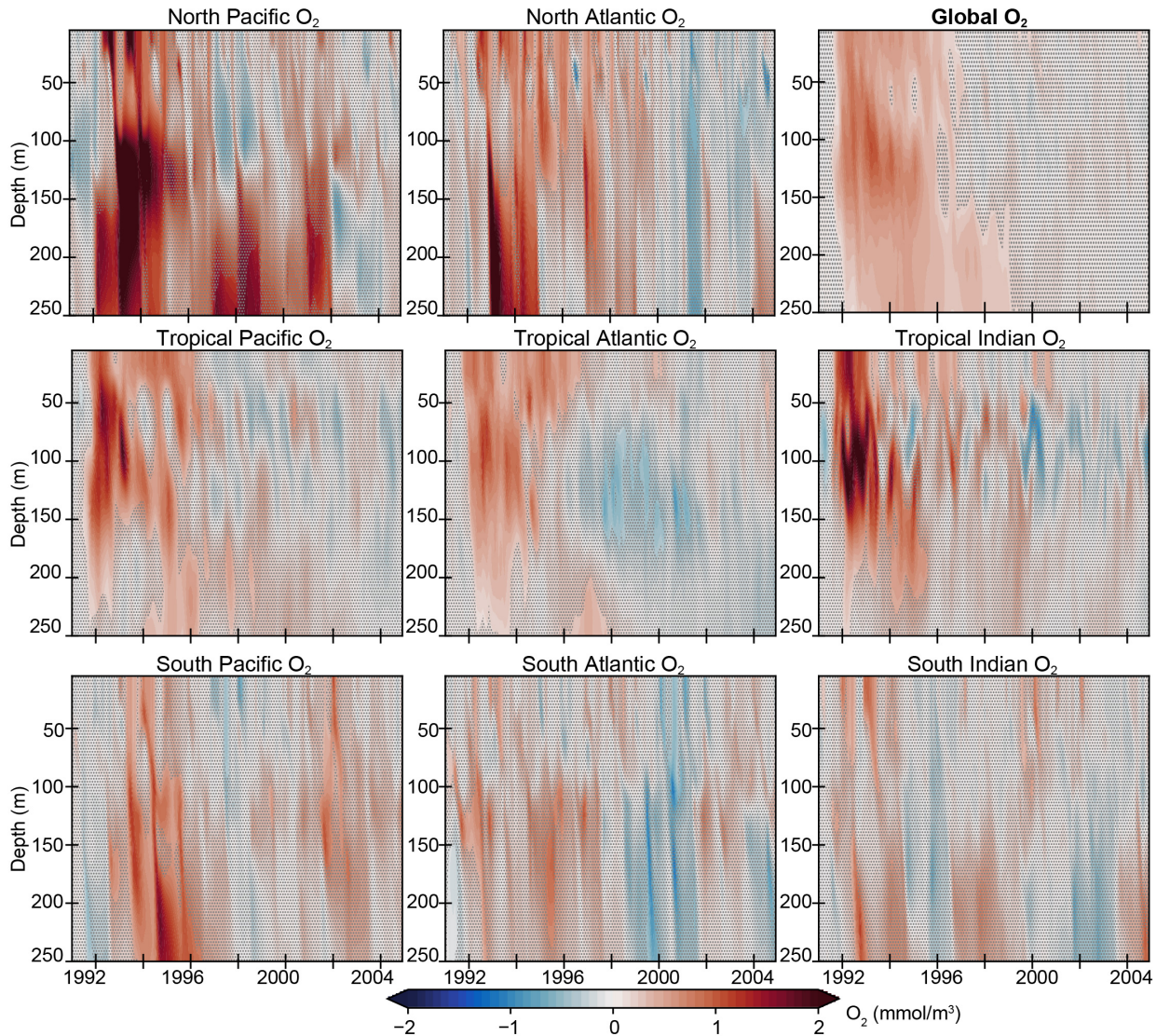
953 **Figure 3.** Globally averaged vertical profile of difference plots (CESM-LE minus CESM-LE-NoPin) for
 954 ensemble mean in a) temperature ($^{\circ}\text{C}$) b) $[\text{O}_2]$ (mmol/m^3), and c) $[\text{DIC}]$ (mmol/m^3). Stippling indicates
 955 time/depth where differences are not significant at the 95% confidence level [Deser *et al.*, 2012a]. Positive
 956 anomalies (warm colors) indicate greater values with the eruption of Pinatubo while negative anomalies (cool
 957 colors) indicate lower values with the eruption. Full model time period available in Figure S3.



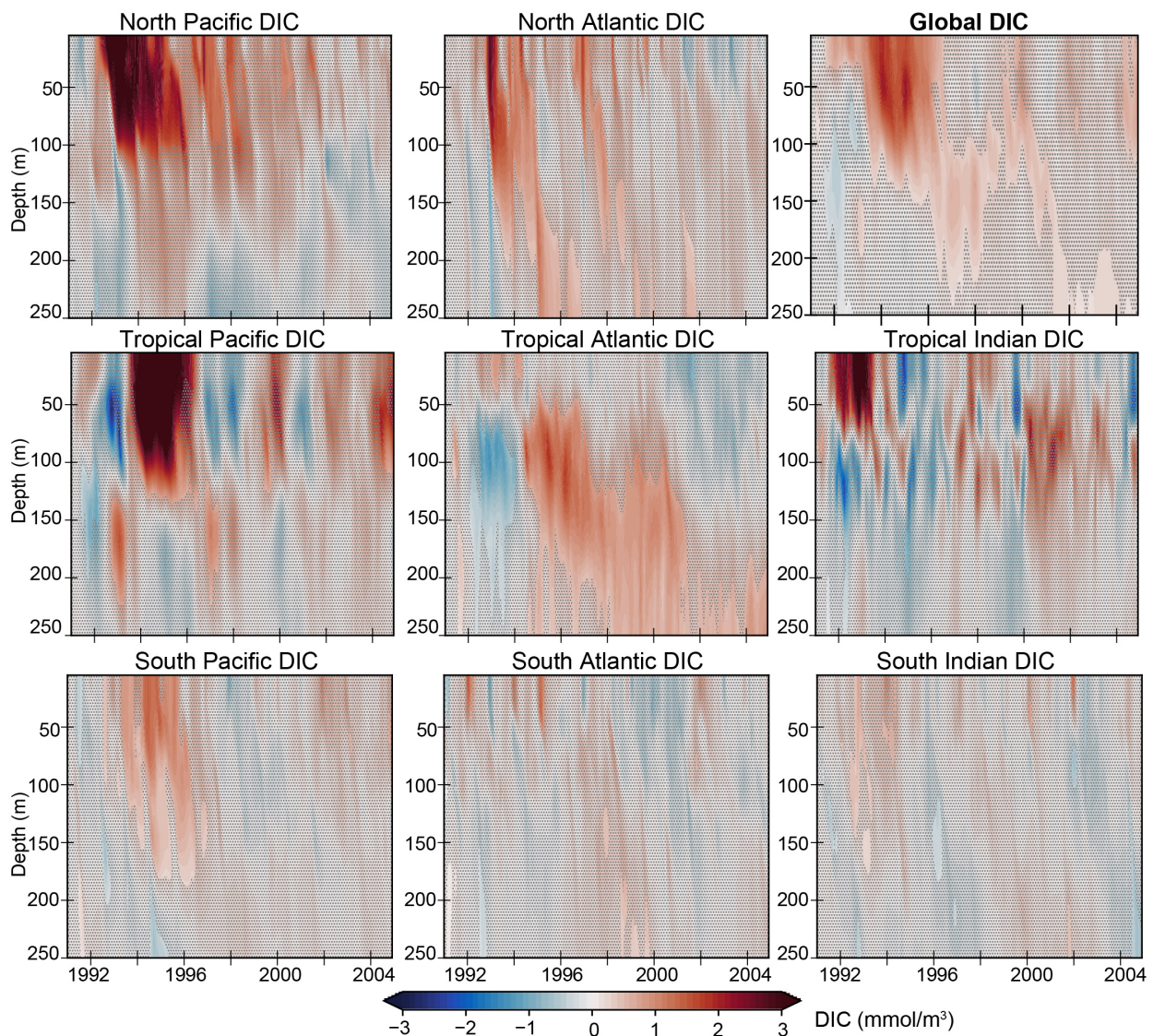
958 **Figure 4.** Evolution of annual mean anomalies (CESM-LE minus CESM-LE-NoPin) sea surface tem-
 959 perature (SST) and maximum mixed layer depth (maxMLD) during the first five years following the June
 960 1991 eruption of Pinatubo: Year 0 (July 1991-June 1992), Year 1 (July 1992-June 1993); Year 2 (July 1993-
 961 June 1994); Year 3 (July 1994-June 1995); Year 4 (July 1995-June 1996). SST anomalies are calculated by
 962 removing the seasonal cycle and annually averaging over respective months. Positive anomalies (warm col-
 963 ors) indicate warmer temperatures and deeper maximum mixed layer depths with the eruption of Pinatubo.
 964 Stippling indicates areas without significant difference between the two ensembles at 2σ [Deser *et al.*, 2012a].



965 **Figure 5.** Evolution of annual mean anomalies (CESM-LE minus CESM-LE-NoPin) depth integrated O₂
 966 (top 1000m) and DIC (top 250m) concentrations during the first five years following the June 1991 eruption
 967 of Pinatubo: Year 0 (July 1991-June 1992), Year 1 (July 1992-June 1993); Year 2 (July 1993-June 1994);
 968 Year 3 (July 1994-June 1995); Year 4 (July 1995-June 1996). Anomalies are calculated by removing the sea-
 969 sonal cycle and annually averaging over respective months. Positive anomalies (warm colors) indicate greater
 970 depth-integrated O₂ or DIC with the eruption of Pinatubo. Stippling indicates areas without significant
 971 difference between the two ensembles at 2σ [Deser et al., 2012a].



972 **Figure 6.** Regionally averaged vertical profile of difference (CESM-LE minus CESM-LE-NoPin) plots for
 973 ensemble mean O_2 inventory (mmol/m^3). Separations are made for the Pacific, Atlantic, and Indian basins
 974 into northern ($>30^\circ\text{N}$), tropical ($30^\circ\text{N}-30^\circ\text{S}$), and southern sections ($<30^\circ\text{S}$) while the global profile is shown
 975 in the top right panel. Stippling indicates time/depth where differences are not significant at the 95% confi-
 976 dence level [Deser *et al.*, 2012a]. Positive anomalies (warm colors) indicate greater oxygen inventory values
 977 with the eruption of Pinatubo while negative anomalies (cool colors) indicate lower oxygen with the eruption.
 978 Similar plot with depth extending to 1000m is available in Figure S8.



979 **Figure 7.** Regionally averaged vertical profile of difference (CESM-LE minus CESM-LE-NoPin) plots
 980 for ensemble mean DIC inventory (mmol/m^3). Separations are made for the Pacific, Atlantic, and Indian
 981 basins into northern ($>30^\circ\text{N}$), tropical ($30^\circ\text{N}-30^\circ\text{S}$), and southern sections ($<30^\circ\text{S}$) while the global profile
 982 is shown in the top right panel. Stippling indicates time/depth where differences are not significant at the
 983 95% confidence level [Deser *et al.*, 2012a]. Positive anomalies (warm colors) indicate greater DIC inventory
 984 values with the eruption of Pinatubo while negative anomalies (cool colors) indicate lower DIC levels with the
 985 eruption. Similar plot with depth extending to 1000m is available in Figure S9.